NWP SAF

*Satellite Application Facility for Numerical Weather Prediction*

Document NWPSAF-MO-VS-018

Version 1.1

3 April 2006

# RTTOVCLD version 8: Independent Assessment

**C J Merchant, O Embury and C P Old**

**The University of Edinburgh**
Institute for Atmospheric & Environmental Science

# RTTOVCLD version 8: Independent Assessment

NWP SAF Document NWPSAF-MO-VS-018

Authors:
**C J Merchant**
**O Embury**
**C P Old**

**The University of Edinburgh**
Institute for Atmos. & Environ. Science
Crew Building
King's Buildings
Edinburgh
EH9 3JN

This documentation was developed within the context of the EUMETSAT Satellite Application Facility on Numerical Weather Prediction (NWP SAF), under the Cooperation Agreement dated 16 December, 2003, between EUMETSAT and the Met Office, UK, by one or more partners within the NWP SAF. The partners in the NWP SAF are the Met Office, ECMWF, KNMI and Météo France.



| Change record | | | |
|---|---|---|---|
| Version | Date | Author / changed by | Remarks |
| 1.0 | 15/02/06 | C. Merchant | Initial draft |
| 1.1 | 03/04/06 | O. Embury | Comments/changes added |
| | | | |
| | | | |
| | | | |
| | | | |

# 1 Introduction

This report describes work undertaken at the University of Edinburgh for the Satellite Application Facility in Numerical Weather Prediction (NWP-SAF) under a contract placed by the UK Met Office.

Management of the mission was undertaken by C J Merchant, with the work described in section 2 performed by C P Old, and the work described in sections 3 and 4 performed by O Embury, all of University of Edinburgh (School of GeoSciences).

The report was commissioned in support of the RTTOV-8 deliverable within the NWP-SAF relating to simulations of cloudy radiances. Fast calculation of cloudy radiances is needed in an increasing number of applications, including cloud detection and retrieval of cloud parameters. The approximations in RTTOV (Cloudy) version 8 (hereinafter RT8C) were expected to correspond to errors that had not been fully assessed and show impact on retrievals was unquantified. This study was therefore commissioned to:

- undertake basic ("beta") testing of the RT8C package [Section 2]
- make comparisons of RT8C with more complete radiative transfer simulations [Section 3]
- and make verifications of simulations against empirical observations [Section 4]

# 2 Basic testing

## 2.1 Scope

This section describes the basic testing of the RT8C package supplied (covering "Work Package 2" in the mission proposal. The objective was to assess the functionality of RT8C as distributed to users, including the accuracy and helpfulness of the support documentation for users, and to make note of discrepancies and recommended improvements to documentation.

The latest version of the Met Office's radiative transfer model RTTOV 8.7 was beta-tested at the University of Edinburgh. The tests run covered installation, compilation, running the NWPSAF test programs and upgrading local software to use RTTOV8.7 (previously we were using RTTOV8.5). The supporting documentation (readme.txt and RTTOV_8_7 Users Guide) was reviewed during the testing.

## 2.2 Overview of Testing

The code was tested on both LINUX and SOLARIS machines, running the following operating system versions respectively:

LINUX: RedHat Enterprise Linux 2.6.9-22.0.1.ELsmp

SOLARIS: SunOS 5.9 Generic_118558-11

Different FORTRAN compilers were used to make the code on the LINUX and SOLARIS machines. The compilers and versions used were:

LINUX: NAGWare Fortran 95 compiler Release 5.0(361)

SOLARIS: Sun Fortran 95 8.1 Patch 117834-03 2005/06/15

The following is a summary of the findings of these tests. For ease of identifying the key findings, omissions, corrections and suggested changes are highlighted by shaded text.

## 2.3 Software Installation and Compilation

The RTTOV8.7 directory structure was extracted from the tar ball onto both the LINUX and SOLARIS systems. All of the subdirectories were created as defined in the list at the end of the *readme.txt* document. Following the instructions in the *readme.txt* document, all four of the *make* options were tested separately on both systems, that is

*make basic*
*make cld*
*make scat*
*make all*.

On the LINUX system the default NAG compiler options in the *Makefile* script were used, and on the SOLARIS the default SUN compiler options were used.

All four cases compiled without errors on both systems. There were a number of standard warnings on both systems these were associated with unused variables. For the scattering code there some instances where there was a warning for scalars being passed to functions expecting an array. There were also comments about the obsolete and deleted features used in the *lapack.f* F77 code. None of the above warnings produced any problems with the code.

The executable files produced were:

*make basic*: example_fwd.out, tstrad.out and tstrad_rttov7.out

*make cld*: rttovcld_test.out

*make scat*: rttovscatt_test.out

*make all*: example_fwd.out, tstrad.out and tstrad_rttov7.out, rttovcld_test.out, rttovscatt_test.out

The installation and compilation ran successfully on both systems.

## 2.4 Running the Test Programs

The AIRS coefficient files and the scattering MIE files had to be downloaded from the RTTOV87 web site in order to run all of the tests.

(a) test_fwd.ksh

The *mtsat imager* test failed as the *input_mtsat.dat* file is missing from the tar ball.

Either the file *rttov87/data/input_mtsat.dat* should be included in the tar ball, or the *mtsat* test removed from the shell script *test_fwd.ksh*.

All of the 83 other tests worked correctly on both systems and all of the difference files produced by comparing our runs to the NWPSAF output were of zero size as expected.

(b) test_fwd_rttov7.ksh

All of the 72 tests worked correctly on both systems and all of the difference files comparing our runs to the NWPSAF output were of zero size as expected.

(c) test_rttov8.ksh

Tests 3 and 4 (both HIRS N15) produced rttov warnings for ozone values outside the coefficient limits. These produced two extra lines in the **.lst* files containing the following warning messages

rttov warning for profile 1
rttov warning for profile 2

These two lines do not appear in the NWPSAF output files. Nonetheless, the differences in the computed values were of an acceptable level. (Perhaps the NWPSAF runs were carried out with the RTTOV warnings turned off?)

Test 35 produced a series of *bad validity parameter* warnings for all channels. This did not result in any significant differences between our run and the NWPSAF output. (Again, it may be that these same warnings occurred for the NWPSAF run?)

Apart from the above mentioned warnings all of the tests produced output that had an acceptable level of difference when compared with the NWPSAF output, suggesting that the code is working correctly as installed.

(d) test_full.ksh

Tests 8 and 13 aborted as the required coefficient files were not in the *rtcoef_rttov8/* directory where the tests were looking. I tried using the corresponding coefficient files from the *rtcoef_rttov7/* and the *rtcoef_rttov8/fastem3/* directories, but neither produced acceptable results compared to the NWPSAF output. They were both internally robust, i.e. produced sensible results.

We suspect, therefore, that a different set of coefficient files were used by NWPSAF to produce the comparison output files. Either the coefficient files

rttov87/rtcoef_rttov8/rtcoef_noaa_15_amsua.dat
rttov87/rtcoef_rttov8/rtcoef_dmsp_15_ssmi.dat

used by NWPSAF should be included in the tar ball, or tests 8 and 13 should be removed from the shell script *test_full.ksh*.

Test 33 failed as there was neither a coefficient file nor the NWPSAF output file for comparison.

Either the files

rttov87/rtcoef_rttov8/rtcoef_coriolis_1_windsat.dat
rttov87/reftest/tstrad_full_33.lst

should be included in the tar ball, or test 33 should be removed from the shell script *test_full.ksh*.

All other tests ran successfully and produced output **.lst* files with acceptable differences in the computed values compares with the NWPSAF output.

(e) test_rttovcld.ksh

The output from all 9 tests were not identical to the NWPSAF test output, but internally all of the tests gave a good test of equality of norms, with the differences ranging from 0.000 to 0.399 times the machine zero. These values are all considered acceptable. Thus is appears that the *rttov_cld* code was installed correctly.

(f) test_rttovscatt.ksh

The output from all 4 were not identical to the NWPSAF test output, but internally all of the tests gave good a good test of equality of norms, with all the differences equal to 0.000 times the machine zero. It was assumed that the *rttov_scatt* code was installed correctly.

**In summary all of the *rttov8.7* code was installed and compiled correctly on both the LINUX and SOLARIS systems at Edinburgh University using the default compiler options in the *Makefile* script.**

## *2.5 Review of Documentation*

(a) readme.txt

There were two minor comments to make on the readme.txt document.

1. The *readme.txt* file does not mention that the executable files created by the make shell scripts are moved to the *scripts/* directory, and initially it was not clear that they had been moved. It is worth including a line in the *readme.txt* file after the paragraph on running the make file stating that the executables are moved to the *scripts/* directory.

2. The readme.txt file states that the shells to be run are

*tstrad_fwd.ksh*
*tstrad_all.src*
*tstrad_full.ksh*

They are in fact

*test_fwd.ksh*
*test_all.src*
*test_full.ksh*

These file names should be corrected in the *readme.txt* file for consistency.

Other than these two points, the *readme.txt* file gives enough information to install and test the code.

(b) RTTOV_8_7 User Guide

In general the documentation is very clear and very useful for running the standard code. The following are a list of suggested corrections and changes that may improve the document.

Section 2, paragraph 1, last sentence (clarity)

This sentence is a little ambiguous; I assume it means that in the future coefficient files for different sets of pressure levels will be made available. This could be clearly stated.

Section 2.2, paragraph 1, first sentence (clarity)

The phrase "Assuming black, opaque clouds at …" would presumably be more precise if reworded "Assuming black-body clouds …"

Section 5, paragraph 1, second sentence (missing word)

Insert the word 'in' between 'enabled' and '**parkind1**'.

Section 5.2, paragraph 1, near end (clarity)

The ',' and the word 'and' in '**channels, polarisation and lprofiles**' should not be bold, e.g.

'**channels**, **polarisation** and **lprofiles**'

Section2.3, bullet point 6 (inconsistency with web material)

This states that the Planck-weighted coefficients are available from the RTTOV-8 web site. We were unable to identify them anywhere on the site. Are these yet to be included?

Section 4.3, paragraph 2 (inconsistency/omission)

It is stated that sample difference files (i.e. *.diff files) are available in the *reftest/* directory.
This was not the case for the tar ball we receives.

Either the **.diff* files should be included in the tar ball or this statement be removed from the document.

As a general comment there is very little information on implementing the *rttov_cld* and *rttov_scatt* functions, i.e. one bullet point at the end of section 5.4 and a list of the parameters in the Annex.

It would be worth while providing the User with more information, at a similar level to that for *rttov_direct*, on implementing both the *rttov_cld* and *rtov_scatt* functions.

## *2.6 Upgrading Local Software to Use RTTOV8.7*

To test the RTTOV8.7 code in local software, the new version of the code was linked into existing cloud screening code at University of Edinburgh. This code only uses *rttov_direct* and *rttov_k*, so will not give an independent test of the *rttov_cld* and *rttov_scatt* code.

Upgrading the code was a satisfactorily trival process. The cloud screening code was recompiled using the new libraries on both the LINUX and SOLARIS systems. The code compiled without any problems. When the code was run profile limit warnings were produced due to the more robust limit checking in the new version of rttov8. We required to turn these warnings off, and re-ran the code. Brightness temperatures were calculated for 93936 profiles on the LINUX system and 21351 profiles on the SOLARIS systems. On both systems the brightness temperatures calculated using the RTTOV8.7 were identical to those calculated using the old version of the code.

Thus, the process of upgrading existing code to use the new version of RTTOV8 was painless using the source code as it is supplied.

# 3 Assessment of implementation of cloudy calculations

## *3.1 Introduction*

The objective of this WP is to validate RT8C cloudy radiances against an independent radiative transfer code.

As independent code we use DISORT (Stamnes *et al.* 1988; Stamnes *et al.* 2000). In order to ensure the comparison is focussed on the treatment of cloud simulation (and not gas transmittances / surface emissivity) RT8C is used to calculate the profiles of gas transmittance, cloud optical depth and the surface emissivity which are passed to the independent code.

## *3.2 Profile set*

The 60L-SDr profile set (Chevallier 2001) was chosen for the simulations for the RT8C-DISORT comparison. This profile set was chosen as it covers a wide range of atmospheric conditions and includes cloud data. Furthermore the profiles are in a format used by the RT8C example code.

The 60L-SDr profiles are a set of 77 profiles extracted from the ECMWF 40-year re-analysis project and three synthetic profiles (minimum, maximum and mean). Data is provided for 60 model levels and includes all variables necessary for RT8C.

Of the 77 profiles, 5 are correspond to completely clear skies and are not used in this study. Water clouds are present in 67 of the profiles and ice clouds in 64 of the profiles. 59 profiles include both water and ice clouds. Figure 1 shows the distribution of cloud optical thickness around 11 μm for the two cloud phases.

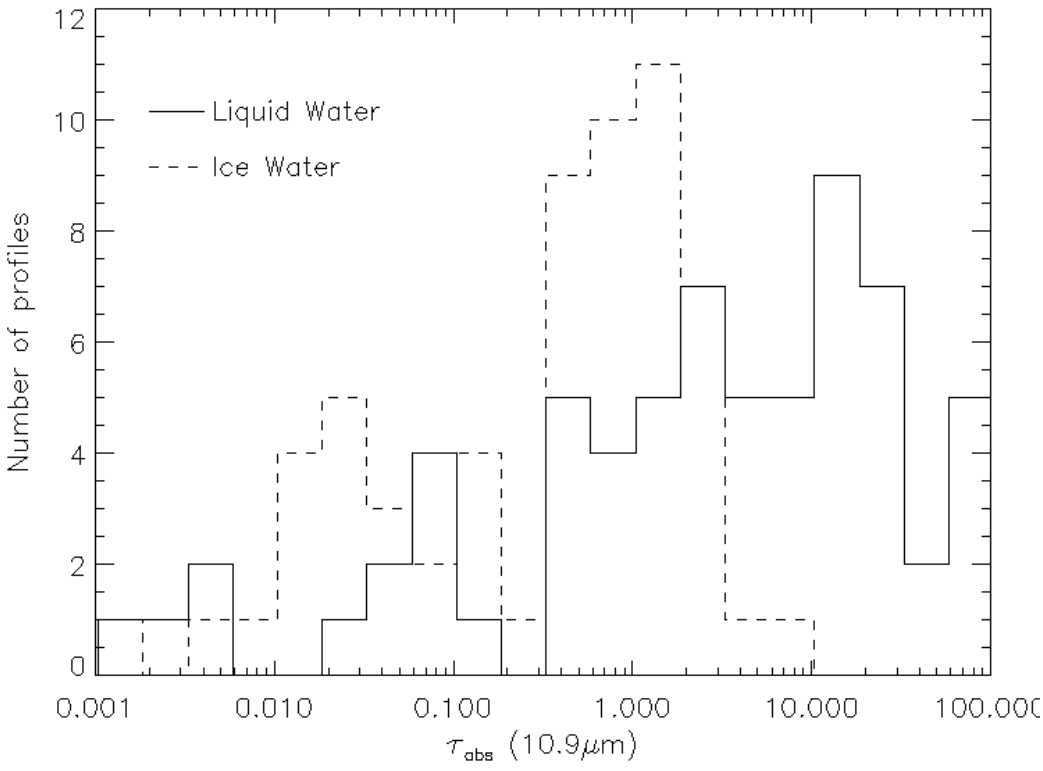


**Figure 1 Distribution of cloud optical thickness (absorption only) in 60L-SDr profile set. Optical thickness here is that calculated by RT8C for the 10.9 micron channel on the AATSR sensor.**

The nomenclature describing the discretization of profiles has different usages of 'level' and 'layer' in the literature for RTTOV, ECMWF, and DISORT. To clarify the usages, Figure 2 shows the relation of the 60 ECMWF model levels to the standard RTTOV pressure levels and the DISORT profile scheme.

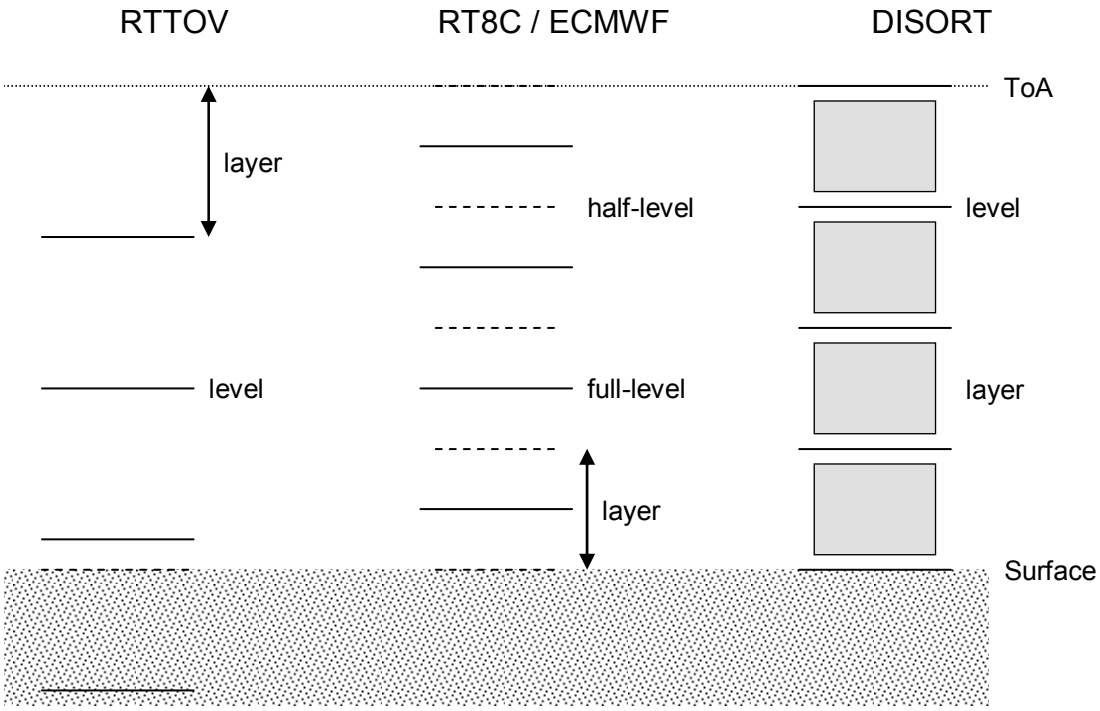


**Figure 2 Comparison of usage describing elements of RTTOV, RT8C, DISORT profiles: the meaning of terms level and layer in the context of the three profile types.**

In summary:

RTTOV: Values of temperature, water vapour are specified at 43 fixed pressure levels. Some levels may be below the surface. A layer is defined between its corresponding level and the level above or ToA for the uppermost layer.

RT8C: Values of temperature, water vapour specified at 60 model levels or "full-level" pressures. Each full level is the mid-point of the two adjacent "half-levels" which run from the ToA to the surface. Layers defined between half-level pressures – i.e. such that the full-level is in the centre of the layer.

DISORT: Optical properties (optical depth, single scattering albedo) specified for any number of layers. Temperature specified at the level (or layer interface) between each layer. DISORT levels are equivalent to RT8C/ECMWF half-levels.

## *3.3 RT8C calculation of cloudy radiances*

It is useful to review the calculation of cloudy radiances in RT8C before describing the equivalent procedures in the independent model.

RT8C uses a multilayer grey-body scheme with a maximum-random overlap assumption to calculate cloud affected radiances (Chevallier *et al.* 2001). In the grey-body approach clouds are assumed to be absorbing only, scattering is ignored, and this allows the total radiance to be expressed as a linear combination of the clear-sky radiance and black-body cloud radiances (as calculated by standard

RTTOV). RT8C does cloudy calculations on user-defined levels (although clear-sky calculations are performed by standard RTTOV requiring that profiles must also be supplied on the standard 43 RTTOV levels) so the RT8C level/layers are the same as the ECMWF profiles (see Figure 2) in this study.

Figure 3 summarises the procedure for the RT8C calculation of cloudy radiances, and Figure 4 shows which FORTRAN source file performs each step.

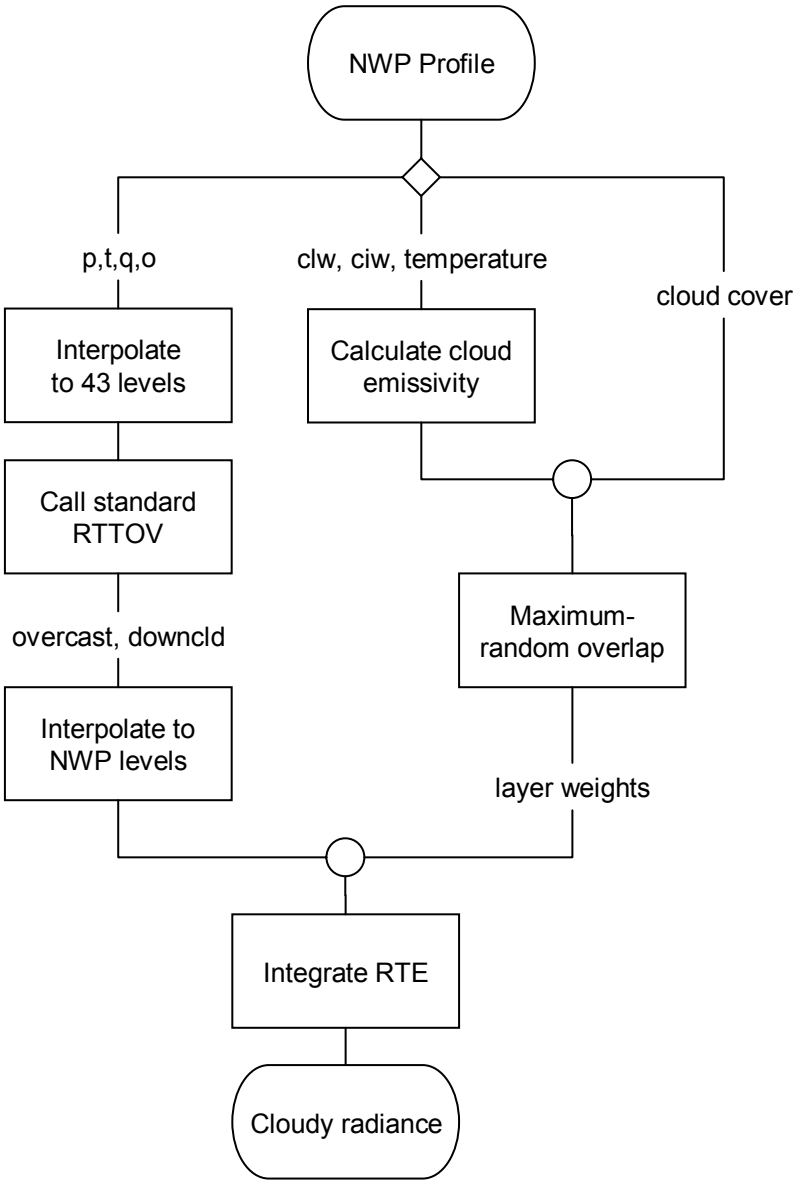


**Figure 3 Flowchart summarising RT8C calculation of cloud affected radiances. p,t,q,o indicates atmospheric profile of pressure, temperature, water vapour, and ozone respectively. clw and ciw are cloud liquid water and cloud ice water.**

rttovcld_test.F90 (or external program)

**Reads NWP profile**

**Interpolates NWP profile to 43 RTTOV levels (rttov_intex.F90)**

rttov_cld.F90

**Calculate gas absorption and black-cloud radiances (rttov_direct.F90)**

**Interpolate overcast, downcld to NWP levels**

rttov_emiscld.F90

**Calculate liquid and ice water path (rttov_intex.F90)**

**Calculate particle radius**

**Lookup single scattering properties**

**Calculate cloud emissivity**

rttov_aitosu.F90

**Calculate layer weights using maximum-random overlap assumption**

**Integrate RT equation**

**Convert radiance to brightness temperature (rttov_calcbt.F90)**

**Figure 4 Structure of RT8C program showing when each step from Figure 3 is performed.**

The interpolation to 43 levels is done before the main RT8C program (rttov_cld.F90) is called, but in this study it is necessary to view this as part of the RT8C process.

After interpolation, the standard RTTOV model (rttov_direct.F90) is called to calculate the 'overcast' and 'downcld' arrays. These are the ToA and surface radiances for a single layer of black cloud (i.e. the cloud is modelled as a perfectly emitting black body) in each of the 43 RTTOV levels accounting for atmospheric absorption and emission above/below the cloud altitude. The overcast/downcld arrays correspond to clouds on each of the standard RTTOV levels and must be interpolated back to the RT8C/ECMWF levels.

Next the cloud emissivity is calculated for each layer which is later used as a weight in defining the effective cloud fraction. This is done in rttov_emiscld.F90 which first calculates the cloud liquid/ice water path in each layer and the absorption coefficient ( $k$ ) for both liquid and ice clouds. The absorption coefficient depends on both the wavelength and the cloud particle effective size. Water clouds are assumed to have an effective radius of 10 μm over land and 13 μm over oceans. For ice clouds there are various parameterisations of the effective diameter. Here only the default (the Ou Liou parameterisation) is used. Once the particle size has been chosen, the absorption coefficient is retrieved from look-up tables (see Hu and Stamnes (1993) for information on the water cloud tables, and Baran and Francis (2004) for details on the ice cloud calculations). The cloud optical thickness is now given by:

$\tau_{liq} = \text{lwp} \times k_{liq}$ and $\tau_{ice} = \text{iwp} \times k_{ice}$

where lwp/iwp is the cloud liquid/ice water path. The emissivity of the cloud layer is then:

$$\varepsilon = 1 - \exp\left(\frac{-\tau_{liq} - \tau_{ice}}{\cos(\theta)}\right)$$

The emissivity calculation assumes that cloud completely fills each layer in the horizontal direction. In order to account for partial cloud cover the cloud emissivity is multiplied by the cloud fraction ( $N$ ) to give an effective cloud fraction:

$$N_{\varepsilon} = N\varepsilon$$

The maximum-random overlap assumption describes the distribution of cloud in partially cloud layers ( $N < 1$ ). In this approach vertically adjacent clouds are assumed to have maximum horizontal overlap, and non-adjacent clouds are assumed to have random horizontal overlap. This implies that the total cloud fraction from the top of layer j thorough to the bottom of layer k is:

$$N(j,k) = 1 - (1 - N_j) \times \prod_{i=j+1}^{k} \frac{1 - \max(N_{i-1}, N_i)}{1 - N_{i-1}}$$

where $N_i$ is the cloud fraction in layer i. However, this only applies to the cloud fraction, so the method described in Räisänen (1998) is used in RT8C to extend it to include effective cloud fraction. This is implemented in the Fortran subroutine rttov_aitosu which calculates the weight of each blackbody cloud layer, given the emissivity of the cloud layer and the cloud fraction.

Finally the radiative transfer equation is integrated by the Fortran subroutine rttov_cld.

## *3.4 Simulations using DISORT*

We use the Discrete Ordinates Radiative Transfer code (DISORT; Stamnes *et al.* 1988; Stamnes *et al.* 2000) to calculate the reference radiances with which RT8C radiances are compared.

DISORT is a highly accurate plane-parallel radiative transfer program which models thermal emission, scattering, and absorption and a wide variety of boundary conditions including: parallel or diffuse illumination, thermal emissions, and bidirectional reflection. DISORT is a RTE solver only – it takes input profiles of optical depth, single scattering properties, and temperature – performing only the final step in the RT8C process, but in a much more general and accurate manner. This makes DISORT ideal for our testing of RT8C, as we wish to retain the RTTOV calculated gas transmission and only compare the treatment of clouds.

There are several modifications which must be made to the RT8C process before DISORT can be used as the RTE solver. These are shown in Figure 5 and are described in detail below.

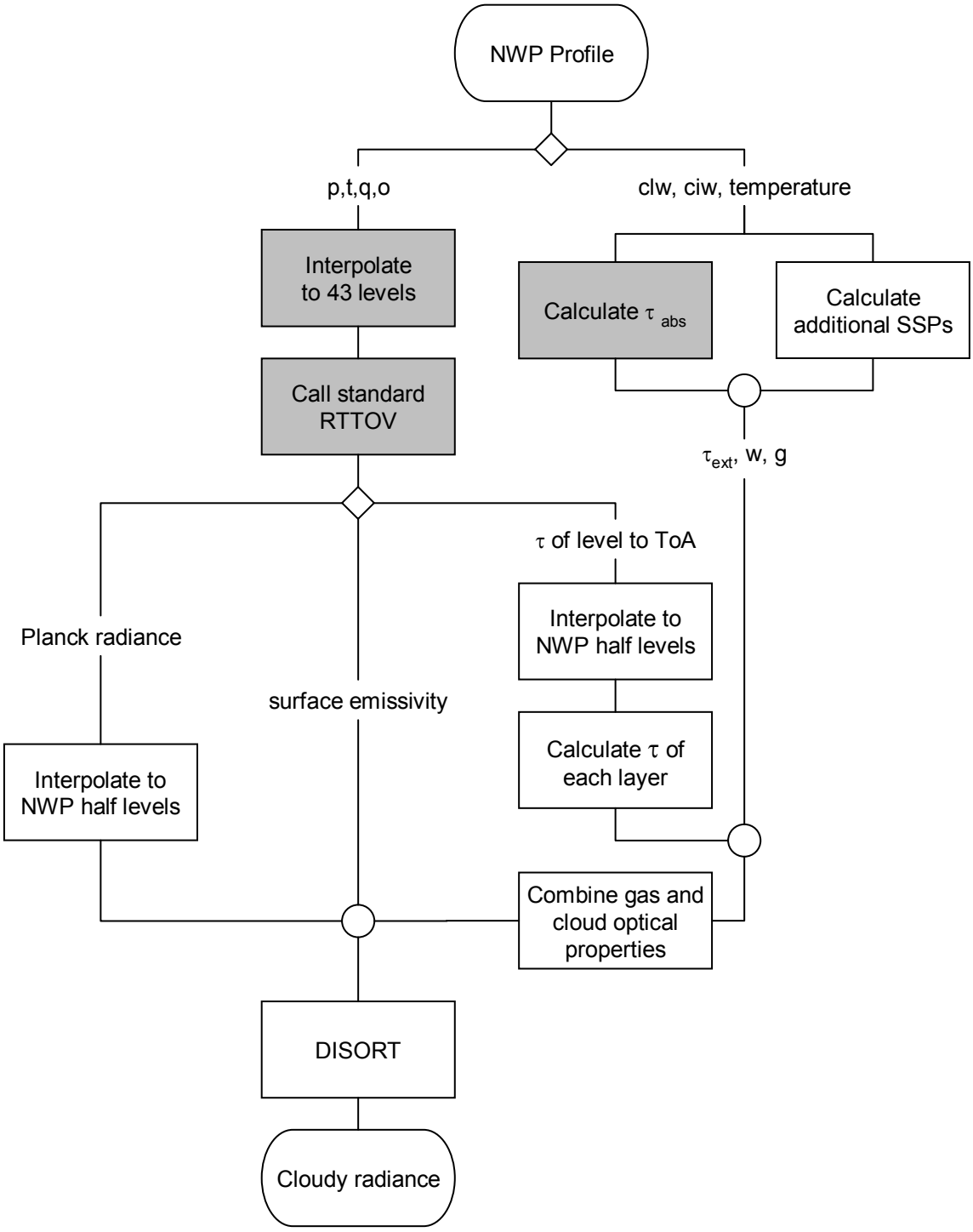


**Figure 5 Flowchart summarising calculation of cloudy radiances using DISORT. τ is optical thickness. Grey highlight indicates steps identical to RT8C process ($\tau_{abs}$ is calculated during the cloud emissivity calculation in RT8C).**

Firstly, the input to DISORT comprises the optical depth, single scattering albedo, and scattering phase function for each atmospheric layer, and the temperature of the interface (level) between each layer. See Figure 2 to see how DISORT level/layers relate to RTTOV and RT8C uses. The temperature is not assumed in DISORT to be constant throughout the layer – instead the Planck radiance varies linearly with optical depth within the layer. The standard RTTOV model calculates the optical thickness of each RTTOV layer (i.e. between each of the 43 RTTOV levels) $\tau(j)$ for j=1,43. By converting this to the optical depth of each RTTOV level (T($j$), i.e., the slant optical path from the level to ToA at zenith angle $\theta$):

$$\mathrm{T}_\theta(j) = \sum_{i=1}^{j} \tau_\theta(i)$$

we can then interpolate this to the optical depth at the NWP half-level pressures (these are the DISORT levels). These half-level optical depths we refer to as $\mathrm{T}'(k)$, where k=1,60. The optical thicknesses of the DISORT layers is then:

$$\tau'_\theta(k) = \mathrm{T}'_\theta(k) - \mathrm{T}'_\theta(k-1)$$

Finally the optical thicknesses must be converted to an optical thickness at nadir rather than the satellite zenith angle using:

$$\tau'_0(k) = \tau'_\theta \cos(\theta)$$

Where calculations are required at a number of satellite zenith angles, it is not sufficient to take the RTTOV calculations at nadir and use an analogous equation, because RTTOV parameterizes the effect of non-monochromatic radiative transfer such that $\tau_0(j) \neq \tau_\theta(j)\cos(\theta)$. This also means it is necessary to rerun DISORT at each zenith angle of interest rather than using its ability to output results at multiple angles in a single run.

As DISORT's levels correspond to the interfaces between the computational layers, it might also seem appropriate to interpolate the temperature profile to the NWP half-level pressures. However, in order to maintain maximum consistency with RT8C, we instead interpolate the RTTOV-level Planck radiances (as calculated by rttov_calcrad – not the blackbody cloud radiances which include atmospheric emission) and modify DISORT to accept these radiances instead of the DISORT-level temperatures. This is equivalent to forcing DISORT to use the same band-corrected Planck function and temperature interpolation method as RT8C, and thus interpolation errors between the two are minimised. The potential errors introduced by interpolation to and from the 43 RTTOV levels are given later.

For the lower boundary it is possible to specify a full bidirectional reflectance function, or assume a simple isotropically reflecting surface (Lambertian surface). It was found that using the Lambertian assumption with albedo set to one minus the surface emissivity (as calculated by RTTOV) was sufficiently accurate (see clear-sky comparison results). Using a full bidirectional reflectance function is unwarranted given the zenith angle dependence of the full atmospheric optical depth.

Next the cloud optical properties are calculated. The rttov_emiscld subroutine already calculates the absorption optical thickness of each cloud layer due to water and ice clouds. To these we add two further optical properties: single scattering albedo (ω) and the asymmetry parameter (g). For water clouds the single scattering albedo is already calculated by rttov_emiscld so it was only necessary to add the asymmetry parameter tables, which we take from Hu and Stamnes (1993). For ice clouds, ω and g are interpolated from additional tables provided by Baran (personal communication, reproduced as Appendix A). The extinction optical depth (used by DISORT) is related to the absorption optical depth by:

$$\tau_{ext} = \frac{\tau_{abs}}{1-\omega}$$

Finally, the optical properties of clear-sky, water clouds and ice clouds must be combined to give a single set of optical properties for each layer.

$$\tau_{ext} = \sum \tau_{ext}(i) \qquad \text{i = clear-sky, water cloud, ice cloud}$$

$$\omega = \frac{\sum \omega(i)\tau_{ext}(i)}{\sum \tau_{ext}(i)}$$

$$g = \frac{\sum g(i)\omega(i)\tau_{ext}(i)}{\sum \omega(i)\tau_{ext}(i)}$$

In addition to the modification to DISORT mentioned above, it was necessary to increase the maximum number of computational layers to 60 so 60L-SDr profiles could be processed.

## *3.5 Interpolation to RTTOV levels*

As mentioned in the previous section the interpolation of temperature profiles from NWP levels to RTTOV levels (converting to radiances) and back to NWP levels can introduce errors. In some rare cases this can lead to errors of up to 1 K in the temperature profile, if the profile includes a strong temperature inversion which peaks between two RTTOV pressure levels. Figure 6 shows one such profile. The original profile is on the 60 ECMWF model levels and the interpolated profile on the 43 RTTOV pressure levels. The profiles are closely matched except at the minimum of the temperature inversion where the model level lies between two RTTOV levels. The crosses show the values taken when the profile is interpolated back to the original model levels – the largest error is now approximately 1 K.

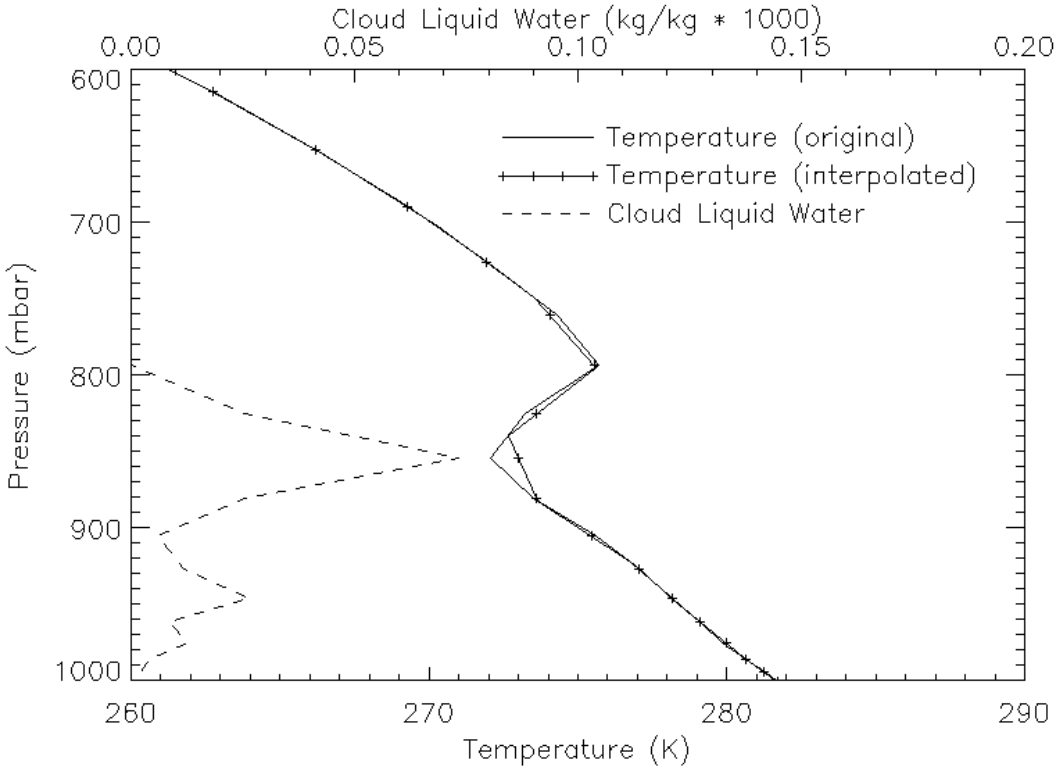


**Figure 6 Atmospheric profile where interpolation to RTTOV pressure levels causes errors of ~1 K. Solid line shows temperature on original NWP levels. Solid line with crosses shows temperature profile on RTTOV levels (crosses indicate NWP pressure levels). Dashed line shows associated cloud liquid water profile.**

The same effect can occur at the temperature maximum of the inversion. This is of less importance to the ToA radiance, however, because clouds tend to be associated with the level of the temperature minimum rather than the maximum (capping of clouds).

Our version of DISORT uses Planck radiances interpolated from the 43 RTTOV levels and so is subject to similar errors of the RT8C model. These errors will not be identical, as DISORT requires the radiances on the half-level pressures not the full-level pressures.

## *3.6 Methods of Maximum-Random Overlap*

RT8C uses the Maximum-Random Overlap (MRO) method of Räisänen (1998) accounting for effective cloud fraction. This will be compared against two alternative implementations of MRO: the stream method (Matricardi 2004) and a stochastic generator (Räisänen *et al.* 2004). Both of these alternative methods work by 'splitting' the cloud cover profile into a number of sub-columns or streams. In each sub-column the cloud fraction is either zero or one on each layer, i.e. a layer is fully cloud or total clear and the sub-column is horizontally homogenous. Although the number of streams can become very large, the method can still be fast as only the integration of the RTE needs to be replicated. The calculation of gas transmittance, surface emission, and cloud emissivity/transmission only need to be performed once. Here we briefly describe and stream and stochastic generator methods.

### 3.6.1 Stream Method

In the stream method the total cloud cover from the ToA to layer j is:

$$N_{tot}(j) = 1 - (1 - N(1)) \times \prod_{i=2}^{j} \frac{1 - \max(N(i-1), N(i))}{1 - N(i-1)}$$

where $N(i)$ is the cloud cover in layer $i$. We can now assign a horizontal extent to each cloud layer if we assume that the cloud is unbroken, i.e., the cloud layer $j$ extends from $N_{tot}(j)$-$N(j)$ to $N_{tot}(j)$. This list of cloud extents (start and end of cloud) is our list of stream edges (after removing duplicates, sorting into ascending order, and adding an upper edge at 1.0 if it is not present). The cloud layers in each stream will be either full or clear, since the cloud extents were used as the stream edges, and thus ToA radiances can be easily calculated. The total ToA radiance is a simple weighted sum of all the streams, with the stream weight equal to its width.

### 3.6.2 Stochastic generator

The Stochastic generator (Räisänen *et al.* 2004) splits the profile into N (here we use 640) sub-columns of equal weight. The layer $j$ in sub-column $k$ is assigned as clear or cloudy by:

$$c_{j,k} = \begin{cases} 0 & \text{for} \quad x_{j,k} \le 1 - N_j \quad \text{(clear)} \\ 1 & \text{for} \quad x_{j,k} > 1 - N_j \quad \text{(cloudy)} \end{cases}$$

where the variable $x$ is generated as follows:

- The uppermost layer is initialised with a random number generator
  $$x_{1,k} = \mathrm{R}_{1,k}(1)$$
  where R($n$) is a random number with values evenly distributed between 0 and $n$.
- Subsequent layers are generated using:
  $$x_{j,k} = \begin{cases} x_{j-1,k} & \text{for} \quad x_{j-1,k} > 1 - N_{j-1} \quad \text{(cloud above)} \\ \mathrm{R}_{j,k}(1 - N_{j-1}) & \text{for} \quad x_{j-1,k} \le 1 - N_{j-1} \quad \text{(clear - sky above)} \end{cases}$$

Note that we have only implemented the MRO generator of Räisänen *et al.* (2004), not the full generator. Unlike the stream method, the stochastic generator produces horizontally broken clouds. Adjacent layers have maximum horizontal overlap, but non-adjacent layers now have truly random overlap (assuming an ideal random number generator).

## *3.7 RT8C – DISORT comparisons*

### 3.7.1 Clear-sky comparisons

An initial comparison of RT8C and DISORT was performed for clear-sky cases to check the DISORT model had been correctly implemented. In this case the results from RT8C are simply the standard clear-sky RTTOV results computed on 43 levels. DISORT was run both on the NWP model levels as described above, and a simplified clear-sky only version operating on the 43 RTTOV levels.

All 77 60L-SDr profiles were used since cloudiness was not required. The AATSR instrument channels were chosen because AATSR includes the three main window channels (3.7, 10.9, and 12.0 microns), and is also the sensor used in Section 4. Four satellite zenith angles were chosen: 0.0°, 48.19°, 60.0°, 66.42° corresponding to equal increments in (plane-parallel approximated) path lengh: sec(θ)=1.0, 1.5, 2.0, 2.5 respectively.

Two statistics are used to compare the ToA brightness temperatures: the 'bias' or mean of differences, and 'spread' or standard deviation of the differences. The difference is always assumed to be RTTOV BT – DISORT BT so that a positive bias indicates the RTTOV values were higher than the DISORT calculated ones.

Table 1 and **Table 2** show the results for DISORT on 43 levels and 60 NWP levels respectively. In all cases there is excellent agreement between RTTOV and DISORT. Both DISORT implementations are consistent indicating that there are unlikely to be significant errors in the RTTOV-DISORT interface. It is only in the 11 and 12 micron channels at high zenith angles (66°) that the bias and spread slightly exceed 0.1K. This is due to RTTOV assuming the atmospheric layers are "optically thin" – it assumes the radiance emitted from a layer is the average of the radiance at the temperature of the levels at the top and bottom of the layer. However, if the layer is not optically thin the upper regions of the layer will contribute more significantly than the lower regions. At higher zenith angles, this optically thin assumption is less valid.

| **Wavelength** | **Zenith Angle** | **0.00** | **48.19** | **60.00** | **66.42** |
|---|---|---|---|---|---|
| **12.04** | **Bias / K** | **-0.06** | **-0.01** | **0.05** | **0.15** |
| | **Std. dev. / K** | **0.05** | **0.04** | **0.05** | **0.13** |
| **10.85** | **Bias / K** | **-0.04** | **-0.00** | **0.04** | **0.10** |
| | **Std. dev. / K** | **0.09** | **0.06** | **0.06** | **0.08** |
| **3.74** | **Bias / K** | **-0.04** | **-0.01** | **0.01** | **0.05** |
| | **Std. dev. / K** | **0.07** | **0.04** | **0.03** | **0.04** |

**Table 1 Comparison of RTTOV (standard) and DISORT (simplified 43 level version) for clear-sky profiles. Bias is mean of RTTOV BT – DISORT BT. Std. dev. is the standard deviation of the same difference.**

| Wavelength | Zenith Angle | 0.00 | 48.19 | 60.00 | 66.42 |
|---|---|---|---|---|---|
| 12.04 | Bias / K | -0.05 | 0.00 | 0.07 | 0.17 |
| | Std. dev. / K | 0.06 | 0.04 | 0.04 | 0.12 |
| 10.85 | Bias / K | -0.04 | -0.01 | 0.03 | 0.11 |
| | Std. dev. / K | 0.11 | 0.06 | 0.07 | 0.08 |
| 3.74 | Bias / K | -0.02 | -0.01 | 0.01 | 0.05 |
| | Std. dev. / K | 0.04 | 0.05 | 0.03 | 0.05 |

**Table 2 Comparison of RTTOV (standard) and DISORT for clear-sky profiles. Bias is mean of RTTOV BT – DISORT BT. Spread is standard deviation of the same.**

### 3.7.2 Cloudy-sky (no scattering)

For the second set of comparisons clouds were included in the atmospheric profiles, but scattering was "disabled" in DISORT, i.e.:

$$\tau_{ext} = \tau_{abs},\ \omega = 0,\ g = 0$$

This means that the DISORT runs replicate the "scattering" approximation embodied in RT8C (to the limit imposed by the effects of having to interpolate profiles differently for the two models). In principle, then, any major discrepancy would raise a question-mark over whether the intended representation of clouds in RT8C had been correctly implemented.

In this comparison, RT8C was run without any cloud overlap scheme because DISORT only supports horizontally homogeneous layers. Any layer where cloud was present was set to have 100% cloud fraction, all other layers had 0% cloud fraction. Profiles were only included in this comparison when they included clouds of the appropriate type.

Table 3, 4 and 5 show the RT8C – DISORT comparison for water clouds, ice clouds, and both respectively. Biases remain low, though slightly larger than the clear-sky case. However, the spreads are noticeably larger: ice clouds have a spread ~0.1K, water clouds have a spread 0.3-0.4K, and both clouds types together have a spread ~0.3K. The behaviour of single phase clouds (entirely liquid or entirely ice) is as expected from the cloud optical thickness distribution shown in Figure 1. For combined phase clouds the total optical depth will be higher than either single phase, but the spread is nonetheless less than the liquid only phase. This is because the ice clouds are generally above the water clouds and "obscure" the effects of the water clouds slightly.

| Wavelength | Zenith Angle | 0.00 | 48.19 | 60.00 | 66.42 |
|---|---|---|---|---|---|
| 12.04 | Bias / K | 0.05 | 0.09 | 0.13 | 0.17 |
| | Std. dev. / K | 0.37 | 0.38 | 0.40 | 0.41 |
| 10.85 | Bias / K | 0.08 | 0.10 | 0.13 | 0.16 |
| | Std. dev. / K | 0.37 | 0.38 | 0.40 | 0.41 |
| 3.74 | Bias / K | 0.03 | 0.05 | 0.07 | 0.09 |
| | Std. dev. / K | 0.28 | 0.32 | 0.35 | 0.36 |

**Table 3 Comparison of RT8C and DISORT (absorption only) for water clouds**

| Wavelength | Zenith Angle | 0.00 | 48.19 | 60.00 | 66.42 |
|---|---|---|---|---|---|
| 12.04 | Bias / K | -0.01 | 0.05 | 0.11 | 0.18 |
| | Std. dev. / K | 0.10 | 0.09 | 0.10 | 0.13 |
| 10.85 | Bias / K | 0.00 | 0.04 | 0.08 | 0.14 |
| | Std. dev. / K | 0.13 | 0.11 | 0.12 | 0.12 |
| 3.74 | Bias / K | -0.02 | 0.01 | 0.03 | 0.05 |
| | Std. dev. / K | 0.05 | 0.07 | 0.08 | 0.09 |

**Table 4 Comparison of RT8C and DISORT (absorption only) for ice clouds**

| Wavelength | Zenith Angle | 0.00 | 48.19 | 60.00 | 66.42 |
|---|---|---|---|---|---|
| 12.04 | Bias / K | 0.08 | 0.12 | 0.15 | 0.19 |
| | Std. dev. / K | 0.30 | 0.28 | 0.29 | 0.29 |
| 10.85 | Bias / K | 0.10 | 0.12 | 0.14 | 0.17 |
| | Std. dev. / K | 0.30 | 0.29 | 0.29 | 0.29 |
| 3.74 | Bias / K | 0.05 | 0.06 | 0.07 | 0.08 |
| | Std. dev. / K | 0.23 | 0.26 | 0.28 | 0.29 |

**Table 5 Comparison of RT8C and DISORT (absorption only) for both water and ice clouds**

To understand the origin of the increased spread, consider Figure 7, which shows plots of bias against cloud optical depth for single phase clouds. For optical thicknesses less than 1.0 all biases are low. As the optical thickness increases above ~5.0 the biases grow larger with a clear trend visible in the water cloud plots. The same effect is less clear in the ice cloud plots as the ice clouds have lower optical depths so there are fewer data points at higher values. These biases are due to the optically thin layer assumption made in RT8C – similar to the same assumption made by RTTOV. RT8C uses the radiance at the model full-level pressure, which corresponds to the centre of the cloud layer. In DISORT, the upper parts of a layer will be more strongly weighted than the lower regions, and the calculated BT will be lower (as temperature is decreasing with altitude) giving a positive bias.

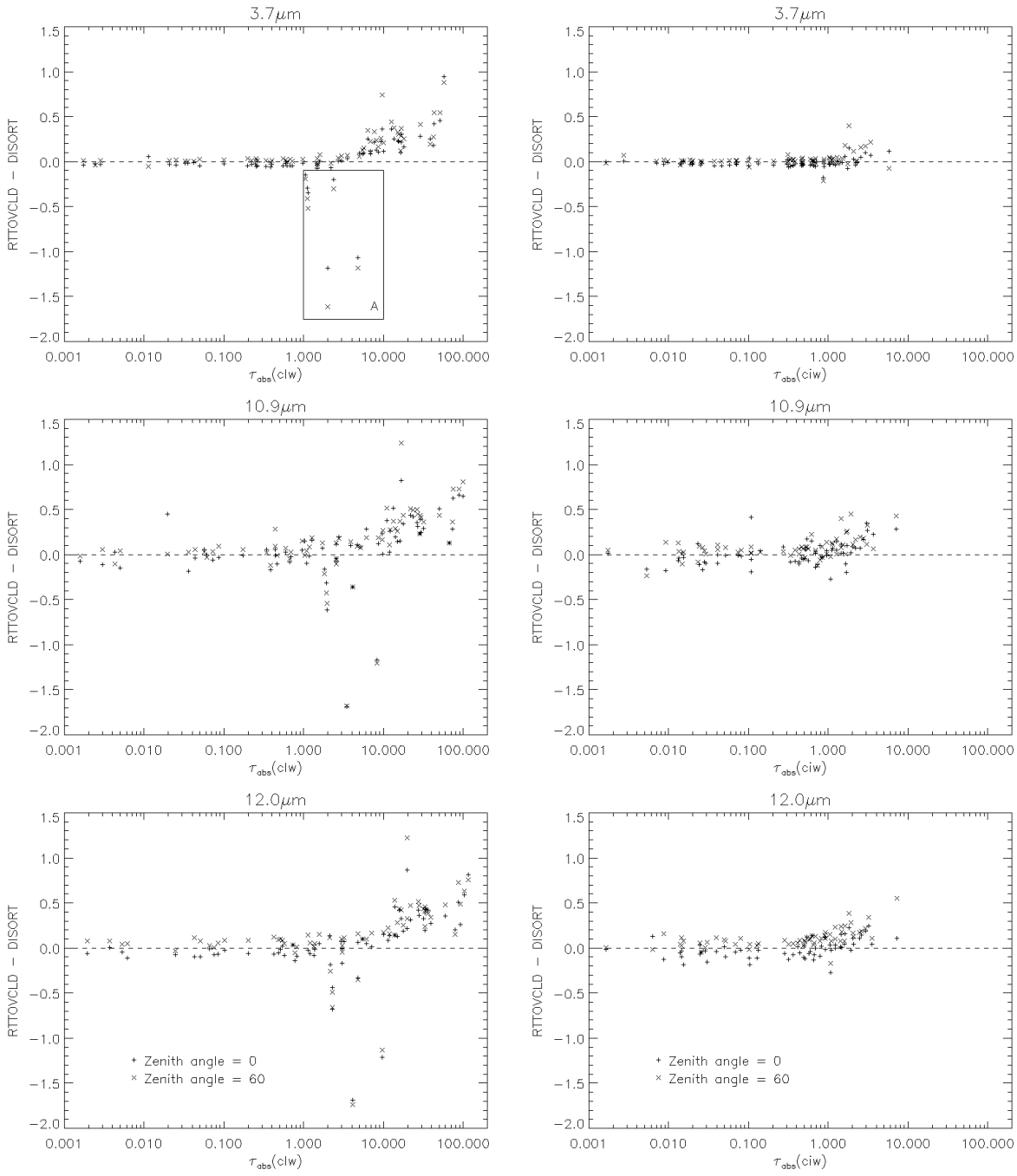


**Figure 7 Plots of bias (RT8C-DISORT [absorption only]) against cloud optical depth for water clouds (left) and ice clouds (right). Optical depth is the absorption-only value at nadir. Clouds producing large negative biases (marked as region A) are all associated with temperature inversions.**

For a few profiles (region A in Figure 7) the opposite effect occurs for water clouds – negative biases indicating the RT8C BT was lower than the DISORT value. This is primarily an artefact of the interpolation to half-level pressure for DISORT rather than full-level pressure for RT8C. In all cases these negative biases are associated with water clouds present on temperature inversions as shown in Figure 8. The layer (or RT8C full-level) with the greatest concentration of cloud is at a local temperature minimum – the adjacent layers both have higher temperatures. In RT8C the entire layer is assumed to be at this minimum temperature, while DISORT assumes the Planck radiance varies linearly between values defined at the layer interfaces (RT8C half-levels). However, as the layer is a local minimum, both interfaces are actually warmer than the 'layer' temperature. The upper interface in particular is warmer than the rest of the layer, and the extra radiance thus emitted is captured by a stronger weighting in DISORT, while the RT8C BTs are too low.

This problem cannot be avoided by "offsetting" the DISORT layers (such that the full level pressures become the layer interfaces and the half-level pressures define the layer centres) because cloud data is required for the layers not for the interfaces. Figure 8 is the most extreme example of this type, corresponding to the largest RT8C-DISORT bias, where the temperature inversion is very strong and the cloud density strongly peaked at the minimum of the inversion.

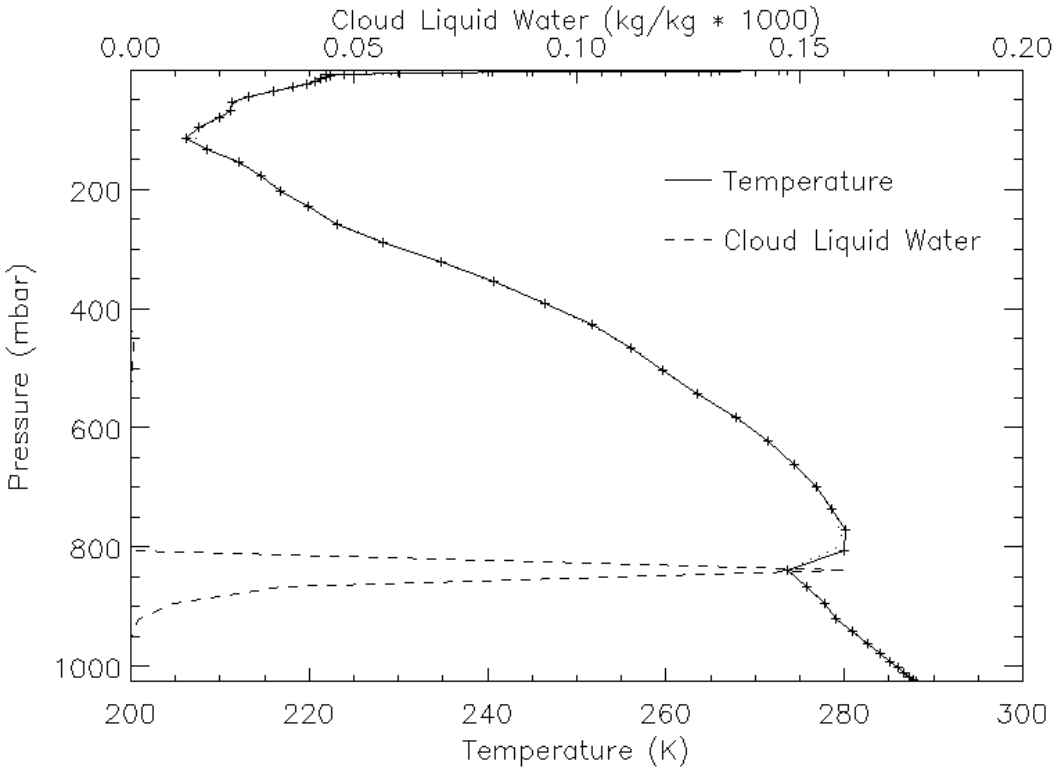


**Figure 8 Example atmospheric temperature profile causing negative bias, as seen in Figure 7. Profile shown on 60 NWP levels, but appears identical on 43 levels (i.e. profile is not affected by 60-43-60 interpolation errors shown in Figure 6)**

(Note that this problem is similar to, but not the same as, the interpolation to RTTOV levels discussed in a previous section. If the temperature minimum lies between two RTTOV levels the interpolation to RTTOV levels will "smooth" the profile and eliminate the bias.)

Figure 9 (left column) shows bias plots for combined phase clouds. The behaviour is similar to water only clouds shown in Figure 7, but slightly weaker and fewer clouds have large negative biases. This corresponds to the overall decrease in bias and spread seen between Table 3 and Table 5, and is due to the ice clouds "obscuring" the radiative effects of the water clouds below, as previously discussed.

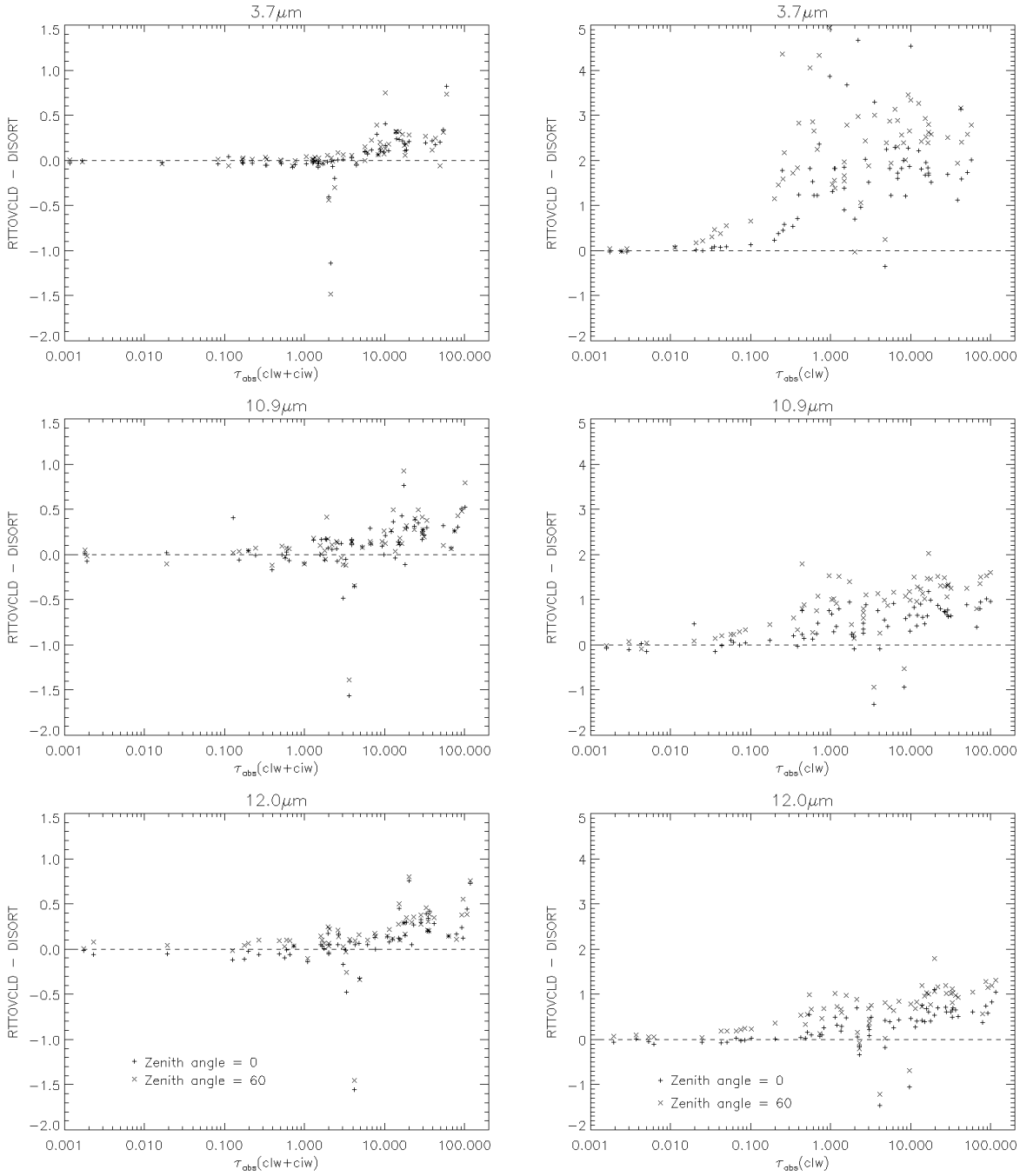


**Figure 9 Plots of bias against cloud optical depth. Left column shows combined water and ice phase clouds with absorption only. Right column shows water clouds with scattering. Optical depth is the absorption-only value at nadir (to preserve comparability across graphs).**

## 3.7.3 Cloudy-sky (scattering included)

For the final set of RT8C-DISORT comparisons scattering was enabled in DISORT by including the single scattering albedo and asymmetry parameter. RT8C was run as previously. These comparisons therefore test the effectiveness of the RT8C "scattering" representation compared to the fuller treatment in DISORT.

Results are shown in Table 6, 7, 8, Figure 9 (right column) and Figure 10.

| Wavelength | Zenith Angle | 0.00 | 48.19 | 60.00 | 66.42 |
|---|---|---|---|---|---|
| 12.04 | Bias / K | 0.28 | 0.44 | 0.61 | 0.80 |
| | Std. dev. / K | 0.42 | 0.45 | 0.50 | 0.53 |
| 10.85 | Bias / K | 0.42 | 0.63 | 0.85 | 1.10 |
| | Std. dev. / K | 0.45 | 0.53 | 0.59 | 0.65 |
| 3.74 | Bias / K | 1.40 | 1.71 | 2.00 | 2.26 |
| | Std. dev. / K | 1.10 | 1.13 | 1.21 | 1.25 |

**Table 6 Comparison of RT8C and DISORT (scattering) for water clouds**

| Wavelength | Zenith Angle | 0.00 | 48.19 | 60.00 | 66.42 |
|---|---|---|---|---|---|
| 12.04 | Bias / K | 0.38 | 0.55 | 0.71 | 0.88 |
| | Std. dev. / K | 0.47 | 0.48 | 0.49 | 0.52 |
| 10.85 | Bias / K | 0.19 | 0.28 | 0.36 | 0.47 |
| | Std. dev. / K | 0.27 | 0.27 | 0.27 | 0.28 |
| 3.74 | Bias / K | 0.51 | 0.63 | 0.56 | 0.40 |
| | Std. dev. / K | 1.06 | 0.96 | 0.59 | 0.75 |

**Table 7 Comparison of RT8C and DISORT (scattering) for ice clouds**

| Wavelength | Zenith Angle | 0.00 | 48.19 | 60.00 | 66.42 |
|---|---|---|---|---|---|
| 12.04 | Bias / K | 0.48 | 0.67 | 0.87 | 1.07 |
| | Std. dev. / K | 0.45 | 0.45 | 0.47 | 0.50 |
| 10.85 | Bias / K | 0.42 | 0.54 | 0.68 | 0.83 |
| | Std. dev. / K | 0.36 | 0.38 | 0.41 | 0.43 |
| 3.74 | Bias / K | 1.48 | 1.63 | 1.67 | 1.66 |
| | Std. dev. / K | 1.19 | 1.21 | 1.08 | 1.08 |

**Table 8 Comparison of RT8C and DISORT (scattering) for both water and ice clouds**

Comparing the statistics of water clouds with scattering (Table 6) against absorption only (Table 3), scattering has only had a small effect on the 11 and 12 micron channels – biases increased by 0.3 to 0.5K and spreads increased by 0.1 to 0.2 K, so the overall RT8C-DISORT differences are about 0.5 K. However, the 3.7 micron channel is affected much more. In the absorption only case, the average RT8C-DISORT bias was smallest for this channel, now it is the largest ranging from 1.4 K to 2.2 K. This reflects the fact that scattering is far more significant for water clouds at shorter wavelengths.

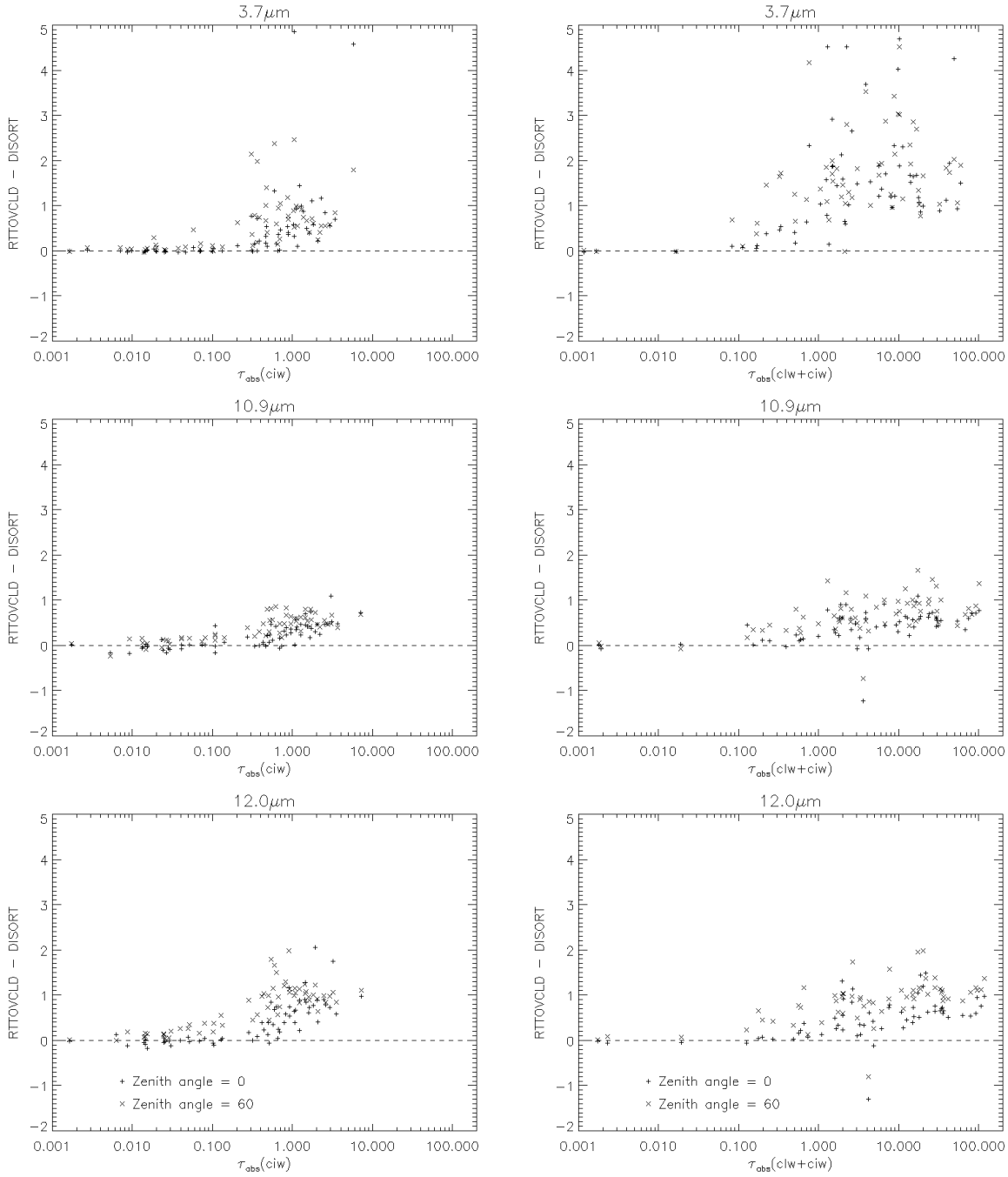


**Figure 10 Plots of bias against cloud optical depth. Left column shows ice clouds with scattering. Right column shows combined water and ice clouds with scattering. Optical depth is the absorption-only value at nadir.**

Comparing the plots of bias in the 3.7 micron channel against optical depth for water clouds with scattering (Figure 9, right column) and absorption only (Figure 7, left column), we see that the RT8C and DISORT results start diverging at much lower cloud optical depths with full scattering activated in DISORT. In the absorption-only case the biases did not increase until the cloud optical depth was between 1 and 10; when scattering is included the cloud optical depth at which the bias begins to increase is between 0.01 and 0.1. The maximum bias found is now much larger, up to 5 K in extreme cases.

Looking at the 11 and 12 micron channels in the same Figures, we see they are influenced far less by scattering. At these longer wavelengths the bias remains low until higher optical thicknesses and the maximum error decreases.

Figure 10 shows bias plots for ice and combined water/ice clouds. Unlike the absorption only case where RT8C-DISORT biases were low for ice clouds due to their low optical thicknesses, the biases are now comparable to those associated with the thicker water clouds. The different scattering properties of water and ice clouds is evident in the bias plots – the 3.7 and 12 micron channel are affected to a roughly equal extent, with the exception of a few outliers, while the 11 micron channel is least affected.

## *3.8 MRO Algorithm Comparison*

Table 9 show statistics (bias, spread, minimum, and maximum) comparing the three MRO implementations. All the biases are low: the stream and stochastic methods being closer to each other than to the default RT8C method. It is only in the 3.7 micron channel that the RT8C method gives results ~0.1 K colder than the other two. However the spreads behave differently and are low (0.4 K) when the RT8C method is compared against the other two, but increased slightly when the stream and stochastic methods are compared (0.6 K at 11 and 12 microns). This can also be seen in the maximum/minimum differences which are greatest between the stream and stochastic methods.

| **Wavelength** | | **Bias / K** | **Spread / K** | **Minimum diff. / K** | **Maximum diff. / K** |
|---|---|---|---|---|---|
| **12.04** | **RT8C – Stream** | **-0.05** | **0.33** | **-1.54** | **0.94** |
| | **RT8C – Stochastic** | **-0.07** | **0.45** | **-3.10** | **1.03** |
| | **Stream - Stochastic** | **-0.03** | **0.62** | **-4.04** | **1.23** |
| **10.85** | **RT8C – Stream** | **-0.07** | **0.35** | **-1.66** | **1.00** |
| | **RT8C – Stochastic** | **-0.08** | **0.48** | **-3.23** | **1.06** |
| | **Stream - Stochastic** | **-0.02** | **0.65** | **-4.23** | **1.34** |
| **3.74** | **RT8C – Stream** | **-0.16** | **0.48** | **-2.46** | **0.34** |
| | **RT8C – Stochastic** | **-0.10** | **0.45** | **-2.19** | **1.17** |
| | **Stream - Stochastic** | **0.06** | **0.48** | **-2.09** | **1.74** |

**Table 9 Comparison of the three Maximum-Random Overlap implementations.**

Although the agreement between the three MRO methods is generally good, there are cases, as can be seen in the maximum/minimum statistics, where there are significant differences (>1 K magnitude). Figure 11 to Figure 15 show five cloud cover profiles with the associated 2D cloud fields where the different MRO methods give markedly different results. ToA BT differences between the methods are shown in Table 10. As explained below, the larger differences arise where there are multiple distinct regions with high cloud coverage.

| Wavelength | Profile | 1 | 2 | 3 | 4 | 5 |
|---|---|---|---|---|---|---|
| 12.04 | RT8C – Stream | 0.94 | -1.54 | -1.14 | 0.01 | 0.36 |
| | RT8C – Stochastic | -3.10 | -0.31 | -0.02 | 1.03 | -0.49 |
| | Stream - Stochastic | -4.04 | 1.23 | 1.12 | 1.03 | -0.85 |
| 10.85 | RT8C – Stream | 1.00 | -1.66 | -1.18 | 0.01 | 0.34 |
| | RT8C – Stochastic | -3.23 | -0.32 | -0.03 | 1.06 | -0.50 |
| | Stream - Stochastic | -4.23 | 1.34 | 1.15 | 1.05 | -0.85 |
| 3.74 | RT8C – Stream | 0.32 | -1.41 | -1.26 | 0.01 | 0.32 |
| | RT8C – Stochastic | -1.77 | -0.30 | -0.17 | 1.17 | -0.46 |
| | Stream - Stochastic | -2.09 | 1.11 | 1.09 | 1.16 | -0.78 |

**Table 10 Differences (in kelvin) between pairs of the three MRO implementations for the five example profiles shown in Figure 11 to Figure 15.**

Figure 11 shows the profile which gave the largest difference between the stream and stochastic methods (4 K at 12 microns) with the RT8C result closer to the stream method (still 1 K difference). Looking at the cloud fields, we see that the total cloud cover from the ToA to any atmospheric layer is the same for both stream and stochastic generators. However, the distribution in layers below the 'visible from above' clouds is different. While satisfying the maximum overlap requirement, the stream method places clouds in such as way as to maximize the cumulative cloud cover from ToA down to a given layer. The stochastic method will also maintain maximum overlap with non-adjacent, but connected, layers. As already noted, when clouds are placed satisfying the random overlap requirement, both methods produce the same result if the cloud is the highest cloud in its own sub-column. However, when a 'randomly' placed cloud is placed underneath another (non-adjacent) cloud layer, the stream method will give maximum overlap with the nearest layer above, while the stochastic generator does give truly random overlap with higher layers. If the clouds were opaque (i.e. black-body) then the different cloud fields would not affect the ToA BTs.

Figure 12 shows a profile where the uppermost level has 100% coverage, but the lower levels do not. As before this constrains the stream cloud field, this time to the extent that it is a 'mirror image' of the cloud cover profile. In the stochastic cloud field, the random distribution of the lower cloud is clear. This profile produced the largest RT8C-stream difference (-1.54 K at 12 microns), however the RT8C-stochastic difference was still 0.31K.

Figure 13 shows another case where the upper most cloud layer covers 100% of the field. The stream method is affected in the same way as before giving a RT8C-stream difference of -1.14K, while the RT8C-stochastic difference is negligible (-0.02 K).

Figure 14 shows a profile which appears to be a relatively straightforward case: cloud extending though many layers but with almost total coverage. Indeed, the RT8C-stream difference is slightly less than 0.01K, but the RT8C-stochastic difference is over 1 K. The cloud fields are also comparable, the significant difference being that the in the stream cloud field, lowest level clouds are not associated with columns with lower cloud top height than in the stochastic assumption..

Figure 15 shows a profile where the stream and stochastic ToA BTs are different by 0.85 K at 12 micron (the stochastic BT being warmer) with the RT8C BT this time about half way between the two. As with

the previous example the stream method has associated the lowest level clouds with lower columns with lower cloud top height, resulting in a cloud field with roughly uniform thickness (in terms of number of layers) everywhere, while the stochastic field ranges from 1 to 13 layers.

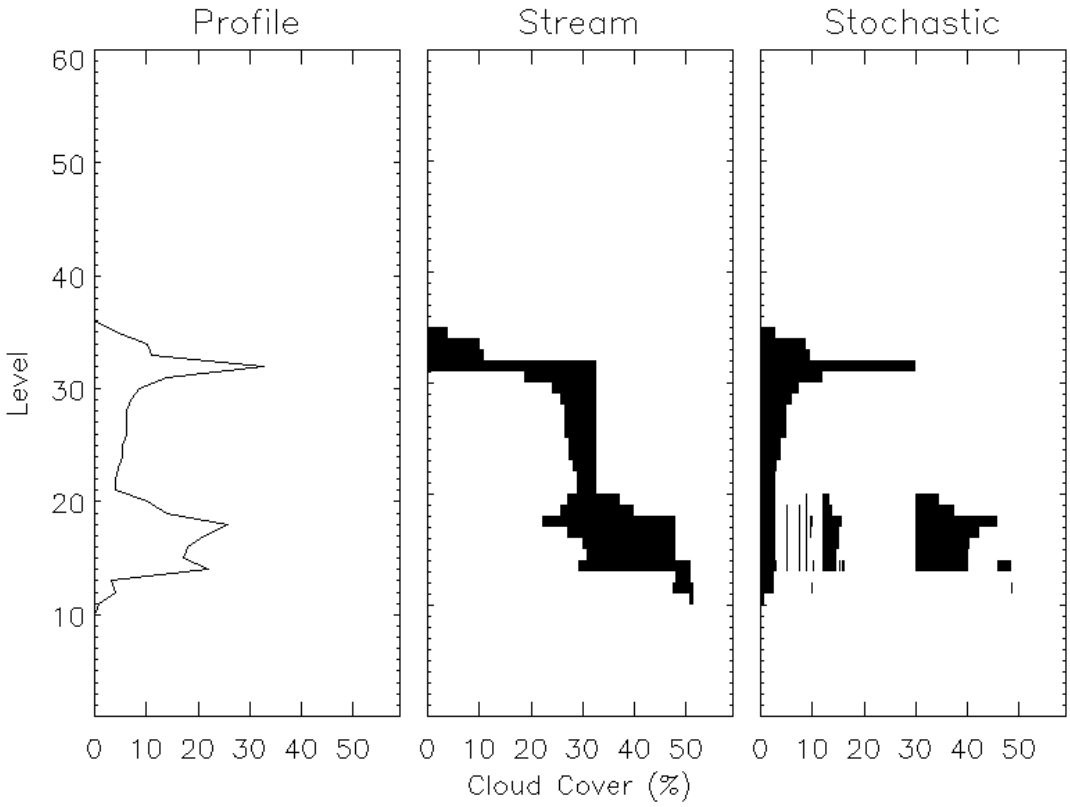


**Figure 11 ECMWF cloud cover profile (%) and corresponding 2D cloud fields generated using Stream and Stochastic methods. Columns in the Stochastic field have been reordered to keep high clouds horizontally adjacent. Differences in ToA BT are shown in Table 10**

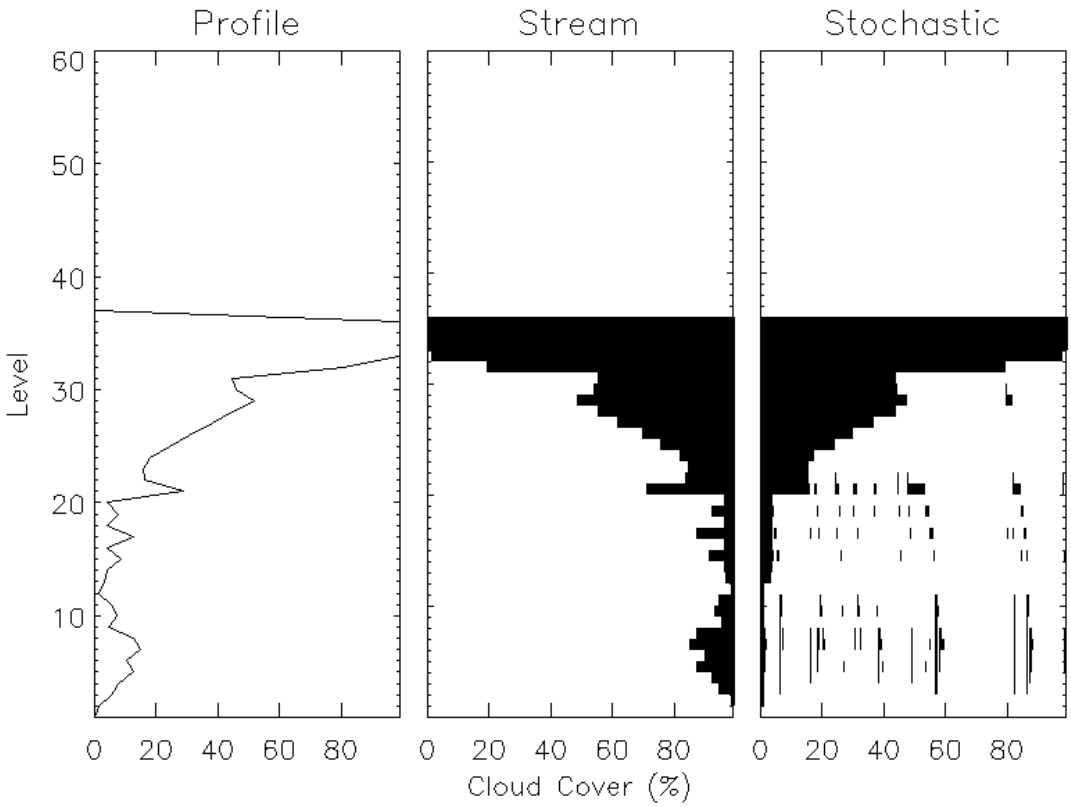


**Figure 12 As Figure 11 for example profile 2**

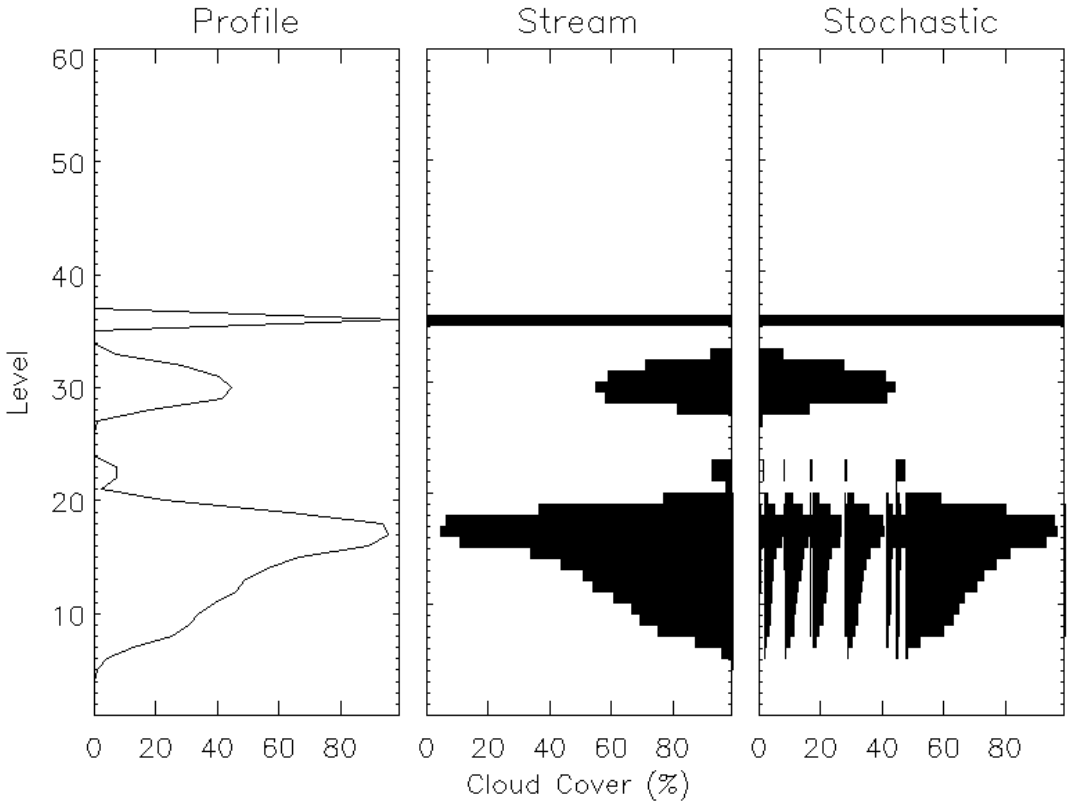


**Figure 13 As Figure 11 for example profile 3**

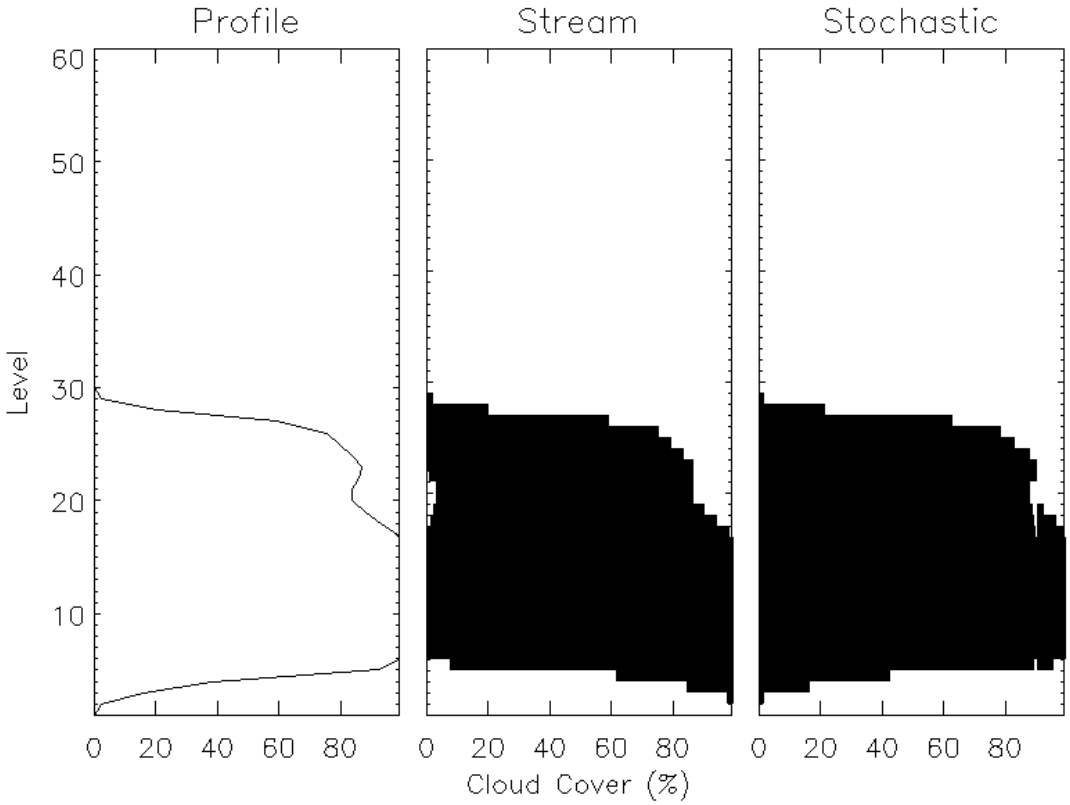


**Figure 14 As Figure 11 for example profile 4**

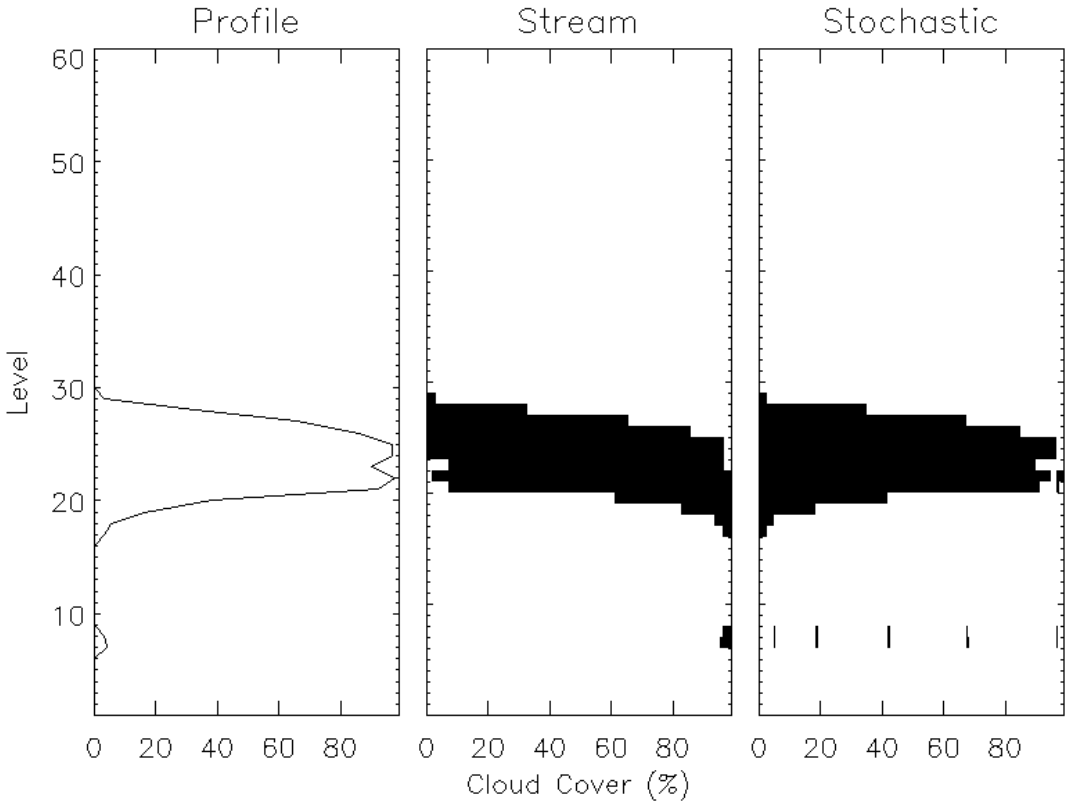


**Figure 15 As Figure 11 for example profile 5**

## *3.9 Summary and conclusions on RT8C-DISORT comparisons*

There are differences between ToA BTs calculated by RT8C and DISORT that range from <0.1 K to several kelvin. These have three causes: the interpolation between different descriptions of atmospheric profiles, the implicit assumption in RTTOV that layers are optically thin, and the neglect of scattering in the RT8C treatment of aerosol.

Some degree of interpolation error is unavoidable when calculations must be performed on a different set of pressure levels to the levels the profile is defined on. However, the effects are generally negligible unless there is a temperature inversion at a level where clouds are present. In the current study the interpolation errors have been separated into two categories.

The first category covers errors associated with the interpolation to 43 RTTOV levels necessary to run the standard RTTOV model. In the rare case that the model level of a temperature minimum lies between two RTTOV levels an error up to ~1 K in the profile is possible. The RT8C-DISORT comparison was designed such that DISORT would be subject to these errors in the same way as RT8C.

The second category covers interpolation errors due to RT8C and DISORT requiring the temperature at different pressures: the layer centre for RT8C and the layer interfaces for DISORT. When the minimum of a temperature inversion falls on a RT8C pressure level, the DISORT ToA BT can be up to 2 K warmer than the RT8C BT.

The RT8C assumption that atmospheric layers are optically thin (i.e., that the radiance leaving the layer is not self-attenuated within the layer) can lead to errors between 0.1 K (under effectively clear-sky conditions) and 0.5 K (for cloudy conditions, where layer optical depths are higher). This becomes more important at higher zenith angles (beyond 60°).

The neglect of scattering causes the largest RT8C-DISORT differences, as one would expect. The differences (effectively, the errors in RT8C) can be significant for clouds of optical depth 0.1 and greater. For water clouds, errors were about 1 K in the 11 and 12 micron channels and 2 to 5 K in the 3.7 micron channel. Ice clouds can cause similar errors even though they generally have lower optical depths: 1 to 2 K in the 3.7 and 12 micron channels and 1 K in the 11 micron channel.

The RT8C radiances could be substantially improved by using a simple “effective emissivity” approximation which would require only minor modifications to the RT8C code (in the rttov_emiscld.F90 file) and some additional single scattering parameters. In this sort of approximation for scattering, the effects of scattering are included in the cloud emission and absorption parameters. This is generally done by scaling the optical thickness of each cloud layer such that scattering forwards is treated as transmission, and scattering backwards is treated as absorption:

$$\varepsilon_{eff} = 1 - \exp\left(\frac{-(1 - f\omega)\tau_{ext}}{\cos(\theta)}\right)$$

where $f$ is the fraction of radiation scattered forwards. (In the absorption only approximation of RT8C $f$=1). A simple function of the asymmetry parameter ($g$) can be sufficient to define $f$. For simulations of aerosol effects in defining (A)ATSR retrieval coefficients, the code RADTRAN (developed at Edinburgh from the RADGEN code of Albin Zavody) uses:

$$f = \frac{1 + g}{2}$$

More complex approaches include that of Chou *et al.* (1999), who use a third order polynomial, and that in RTIASI-5 (Matricardi, 2004), which allows a more precise definition of the phase function than just *g*, and calculates *f* from an integral of the phase function over one hemisphere.

By comparing the RT8C MRO assumption with two other MRO implementations, we have shown that, in most cases, the differences between the three versions of MRO are small. However, under certain conditions which comprised ~10% of the sample used here (such as when there are multiple distinct regions with high cloud coverage) the MRO implementations can lead to BTs that differ by 1 to 4 K.

## *3.10 References (Section 3)*

Chevallier, F., Bauer, P., Kelly, G., Jakob, C., McNally, T., 2001, Model clouds over Oceans as Seen from Space: Comparison with HIRS/2 and MSU Radiaces. J. Climate, 14, 4216-4229.

Chevallier, F., 2001, Sampled databases of 60-level atmospheric profiles from the ECMWF analyses. ECMWF Research Report No. 4.

Chou, M.-D., Lee, K.-T., Tsay, S.-C., Fu, Q., 1999, Parameterization for Cloud Longwave Scattering for Use in Atmospheric Models. Journal of Climate, 12, 159-169.

Hu, Y. X., Stamnes, K., 1992, An Accurate Parameterization of the Radiative Properties of Water Clouds Suitable for Use in Climate Models. Journal of Climate, 6, 728-742.

Matricardi, M., 2004, The inclusion of aerosols and clouds in RTIASI. ECMWF. RTIASI final report.
Räisänen, P., 1998, Effective Cloud Fraction and Maximum-Random Overlap of Clouds: A Problem and a Solution. Monthly Weather Review, 126, 3336-3340.

Stamnes, K., Tsay, S.-C., Wiscombe, W., Jayaweera, K., 1988, Numerically stable algorithm for discrete-ordinate-method radiative transfer in multiple scattering and emitting layered media. Applied Optics, 27, 2502-2509.

Stamnes, K., Tsay, S.-C., Wiscombe, W., Laszlo, I., 2000, A General-Purpose Fortran Program for Discrete-Ordinate-Method Radiative Transfer in Scattering and Emitting Layered Media. DISORT Report v1.1.

# 4 Comparison of RT8C simulations and observations

## *4.1 Objectives*

This section describes work to verify the extent to which RT8C simulations are realistic compared to actual satellite observations. Two innovative means of attempting this verification have been implemented. The first is the simulation using RT8C of cloudy-radiance distributions for comparison with observed climatology of cloudy-radiance distributions. The second is the attempt to simulate specific situations as case-studies.

## *4.2 Comparison of statistical distributions.*

To create an empirical distribution of cloudy radiances, joint probability distributions of cloudy ToA brightness temperature and brightness temperature differences were generated from 10 days of ATSR-2 night-time imagery. The ATSR-2 pixels used were those flagged cloudy by standard ("SADIST") cloud screening and which were surrounded by pixels in a 7x7 box centred of which all were also flagged as cloudy. This is intended to minimize the contribution to partially cloud-filled pixels in the distribution. Data were taken from the 21st to 26th July 1996 and 27th to 30th January 1999 giving approximately 450 million observations in each of the nadir (0 to 22°) and forward (52 to 56°) view zenith angles. From this sample, Figure 16 shows the joint probability distribution of the difference between the BT in 3.7 and 11 µm channels ("BT3-BT11") against BT in the 11 µm channel ("BT11").

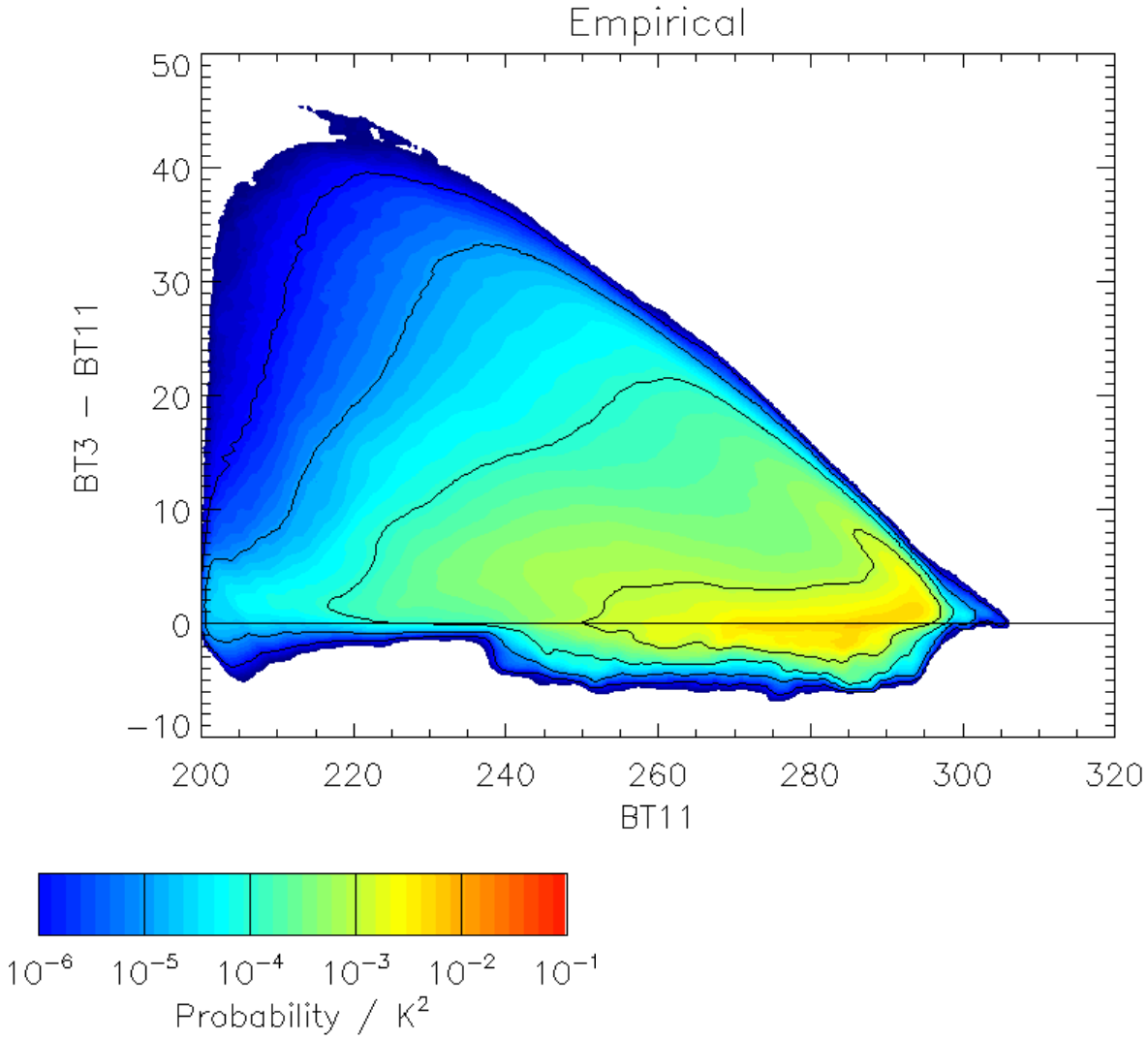


**Figure 16 Joint probability density function of BT3-BT11 difference against BT11 for nadir pixels classified as cloudy by ATSR2 cloud mask.**

This particular distribution is of interest because, of the various combinations one could consider, it gives the best test of the model. Cloudy BTs are much less tightly correlated between the channel at 3.7 μm and the 11 μm (or 12 μm) channel, than between the 11 μm and 12 μm channels, for example. In Figure 16, we can see that a significant fraction of cloudy pixels have differences between the 3.7 and 11 μm channel that exceed 10 K. These are cases where the cloud is semi-transparent (or only partially covers the satellite pixel) such that the observed radiance is a combination of the cloud and surface emitted radiance. Due to the non-linearity of the Planck function any transmitted surface radiance will cause a greater increase in the 3.7 μm BT that the 11 μm or 12 μm BT.

For the simulated distributions the ECMWF 60L-SD profile set (Chevallier 2001) was used. This dataset comprises 13495 profiles (6813 ocean, 1602 land, and 5080 mixed) from which we selected 6982 profiles which were:

- corresponded to at least 25% ocean
- had skin temperature > 273.15 (not frozen)
- had skin temperature < 305.018 (maximum temperature of a 100% ocean profile)
- had non-zero cloud on at least one model level

As the ECMWF profiles correspond to a substantially larger area than the 1 km pixel size of ATSR, and 7000 is insufficient to generate a representative distribution along the lines of Figure 16, the stochastic generator (see section 3.6.2) is used to produce 5000 streams from each profile (i.e., here, N = 5000). Clear-sky streams were discarded leaving approximately 27 million cloudy streams to simulate the distribution. One potential short-coming of this approach is that each stream comprises layers of either 0% or 100% cloud cover (in the section 3.8, multiple streams were averages to simulate the effect of fractional cloud coverage)

RT8C was run using the aggregate ice model and all four ice particle size parameterizations (Ou and Liou (1995), Wyser (1998), Boudala et al. (2002), and McFarquhar et al. (2003)). Simulated joint frequency distributions for these simulates are shown in Figures 17 and 18.

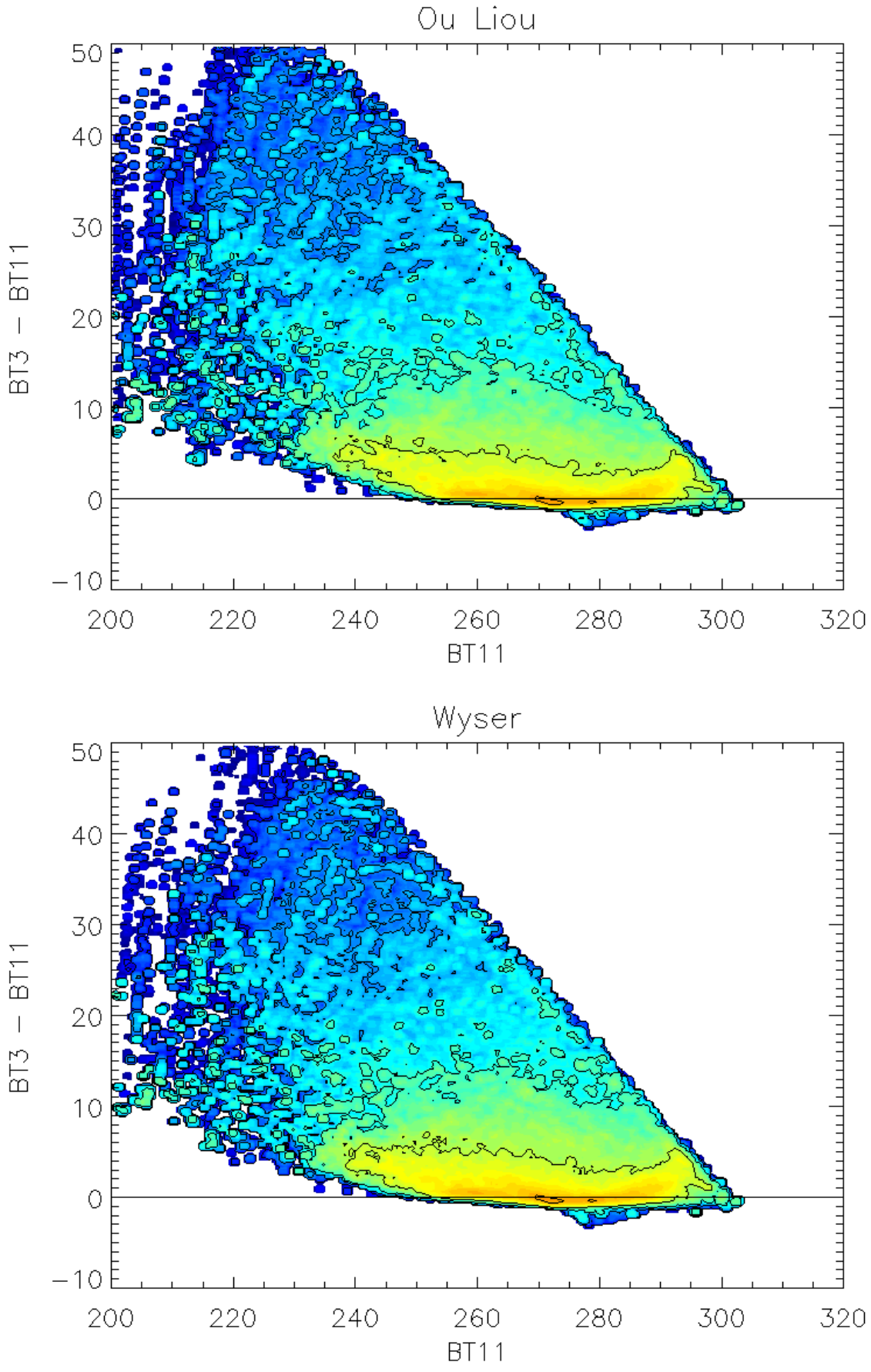


**Figure 17 Joint probability density function of BT3-BT11 difference against BT11 for simulated cloudy radiances generated by RT8C using aggregate ice model. Scale as in** Figure 16**.**

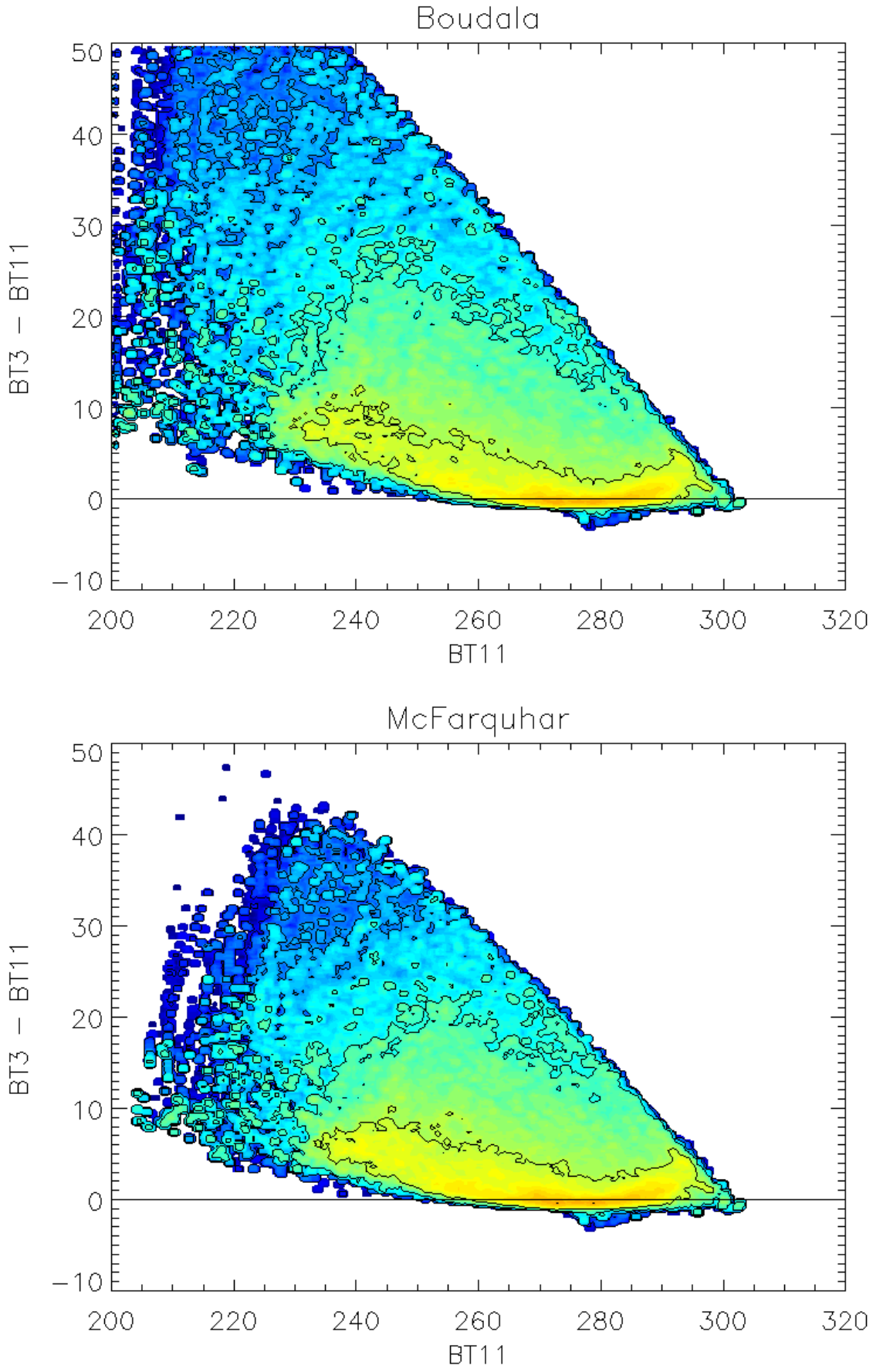


**Figure 18 Joint probability density function of BT3-BT11 difference against BT11 for simulated cloudy radiances generated by RT8C using aggregate ice model. Scale as in** Figure 16**.**

A major difference between the synthetic and the empirical distribution is the abundance of clouds with BT3-BT11 < 0. In the synthetic distributions, few streams produce BT3-BT11 differences more negative than -1 K (the $10^{-3}$ $K^{-2}$ contour is at about -0.5 K), with the extrema having differences of about -3 K. In the empirical distribution, differences down to -3 K are not uncommon (the $10^{-3}$ $K^{-2}$ goes down to about -3 K), and are -6 K for more extreme cases. We interpret this as RT8C failing to simulate fog and low stratus situations properly because of its absorption-only treatment of scattering. As is well known, BT11 > BT3 is one of the features used to identify the presence of fog and low stratus cloud in threshold-based cloud screening tests. Its basis as a test is that clouds have a lower emissivity at 3.7 microns than at 11 microns. However, in the absorption-only approximation used by RT8C, this lower emissivity automatically implies a higher transmissivity in the 3.7 μm channel, so that the warmer surface is more visible in the 3.7 μm channel, which tends to increase the observed brightness temperature. In reality, scattering within the clouds at 3.7 μm means that the extinction within the cloud exceeds the emissivity of the cloud – some surface emission is scattered back down to the surface, and the observed temperatures are lower than RT8C simulates. When scattering is also considered, a cloud can be effectively opaque but still have an emissivity less than one.

There are two cloudy conditions under which BT11>BT3 arises under the absorption only approximation. The first is very thin (semi-transparent) cloud, where the effect is due to the surface emissivity being higher at 11 μm than at 3.7 μm (this effect not being obscured by cloud). This causes the "edge" at BT3-BT11=-0.5 K. The second is where a thick cloud lies on an atmospheric inversion such that the upper layers of the cloud are warmer than the lower layers (or the surface). (This arises in the simulations because of the method of defining the profiles, but, considering the dynamics of cloud capping at inversions, is probably unrealistic in practice.) The depth within the cloud layer from which the radiance originates is deeper (colder) for the 3.7 μm channel than for the 11 μm channel, hence the BT difference. This effect causes the few simulated points around BT11 = 280 K, BT3-BT11 = -3 K.

Simulations to test the above interpretations use the 60L_SDr profile set and selected the 42 profiles that:

- corresponded to at least 25% ocean
- had skin temperature > 273.15
- had skin temperature < 305.018
- satisfied: skin temperature > (maximum atmospheric temperature – 3 K)

which is intended to eliminate the atmospheric inversion situations described above.

The ECMWF cloud data was ignored and replaced with a single layer of water cloud. The cloud level was varied between layer 40 and layer 60 (adjacent to the surface), cloud liquid water content was varied between 0 and 0.001 kg/kg.

Simulations were run using RT8C, DISORT absorption only, and DISORT including scattering. Table 11 shows the minimum observed BT3-BT11 difference, while Table 12 shows the mean change in BT3-BT11 difference between RT8C and DISORT. Results are shown for a range of effective particle sizes. RT8C uses a fixed effective particle size of 13 microns for water clouds, although, as can be seen from the DISORT absorption-only results, varying the particle size would have very little effect on the RT8C results. The minimum RT8C BT3-BT11 value of -0.6 K corresponds to the "edge" seen in the synthetic distribution.

| Particle size (microns) | 15 | 13 | 11 | 9 |
|---|---|---|---|---|
| RT8C | n/a | -0.60 | n/a | n/a |
| DISORT (absorption) | -0.84 | -0.84 | -0.84 | -0.85 |
| DISORT (scattering) | -1.02 | -1.06 | -1.15 | -1.31 |

**Table 11 Most negative BT3-BT11 difference observed using different RTM and liquid particle sizes. Simulations were run using profiles described in text.**

| Particle size (microns) | 15 | 13 | 11 | 9 |
|---|---|---|---|---|
| DISORT (absorption) | 0.13 | 0.07 | 0.01 | -0.06 |
| DISORT (scattering) | -0.27 | -0.37 | -0.53 | -0.77 |

**Table 12 Change in average BT3-BT11 difference between RT8C and DISORT. Simulations were run using profiles described in text.**

Comparing the "DISORT (absorption)" and "DISORT (scattering)" results shows, as expected, that the BT11>BT3 effect from water clouds is enhanced by the scattering processes described above. The magnitude of the effect is dependent on the effective particle size; the smaller the particle size, the larger the BT difference, ~0.4 K for larger particles and ~0.7 K for 9 μm particles.

The main difference between the four ice particle size parameterizations (Ou and Liou; Wyser; Boudala; and McFarquhar) is the maximum BT3-BT11 value produced. In this respect the McFarquhar parameterization most closely matches the empirical distribution, suggesting it may be the most appropriate for RT8C simulations of cirrus (at least under the RT8C absorption-only treatment of scattering).

In all the RT8C simulations, there is a deficit of cases where BT3 ~ BT11 when BT1 reaches 250K and the BT3<BT11 effect is not seen at lower values of BT11. Again, this is due to the neglecting of scattering in the simulations.

Another difference between the RT8C and empirical PDFs is the distribution of the 'most-likely' BTs (i.e. those with probability greater than $10^{-3}$ $K^{-2}$). In the empirical PDFs the $10^{-3}$ $K^{-2}$ contour extends from 255 K to nearly 300 K in the 11 micron channel, the probability peaks at high BTs about 295 K. In all the RT8C PDFs the $10^{-3}$ $K^{-2}$ contours extend to lower temperatures (~240 K in the 11 micron channel) and the probability peaks between 270 K and 290 K. There are two reasons (aside from modelling errors) which are thought to contribute to this.

Firstly, these BTs are very close to the expected clear-sky BTs and hence correspond to partial or very thin cloud. In such cases the underlying SST distribution is visible in the output. As the empirical PDF was generated from ATSR-2 data from only two times in the year the distribution of SST will not necessarily be the same as the 60L-SD profile set.

Secondly, the empirical distribution may still include clear-sky pixels despite the efforts to prevent this. This is because it is known that some failures of the standard cloud screening mask blocks of imagery that are wholly or partly clear.

Figures 19, 20, and 21show joint probability distributions of the BT11-BT12 difference against BT11. Similar to the BT3-BT11 case, the RT8C distributions are generally restricted to positive BT11-BT12 differences. In the empirical distribution, negative BT11-BT12 differences are observed, but are of much lower probability than negative BT3-BT11 differences. The McFarquhar model for ice particles fits the maximum BT11-BT12 less well than the other models, in contrast to the BT3-BT11 difference mentioned above.

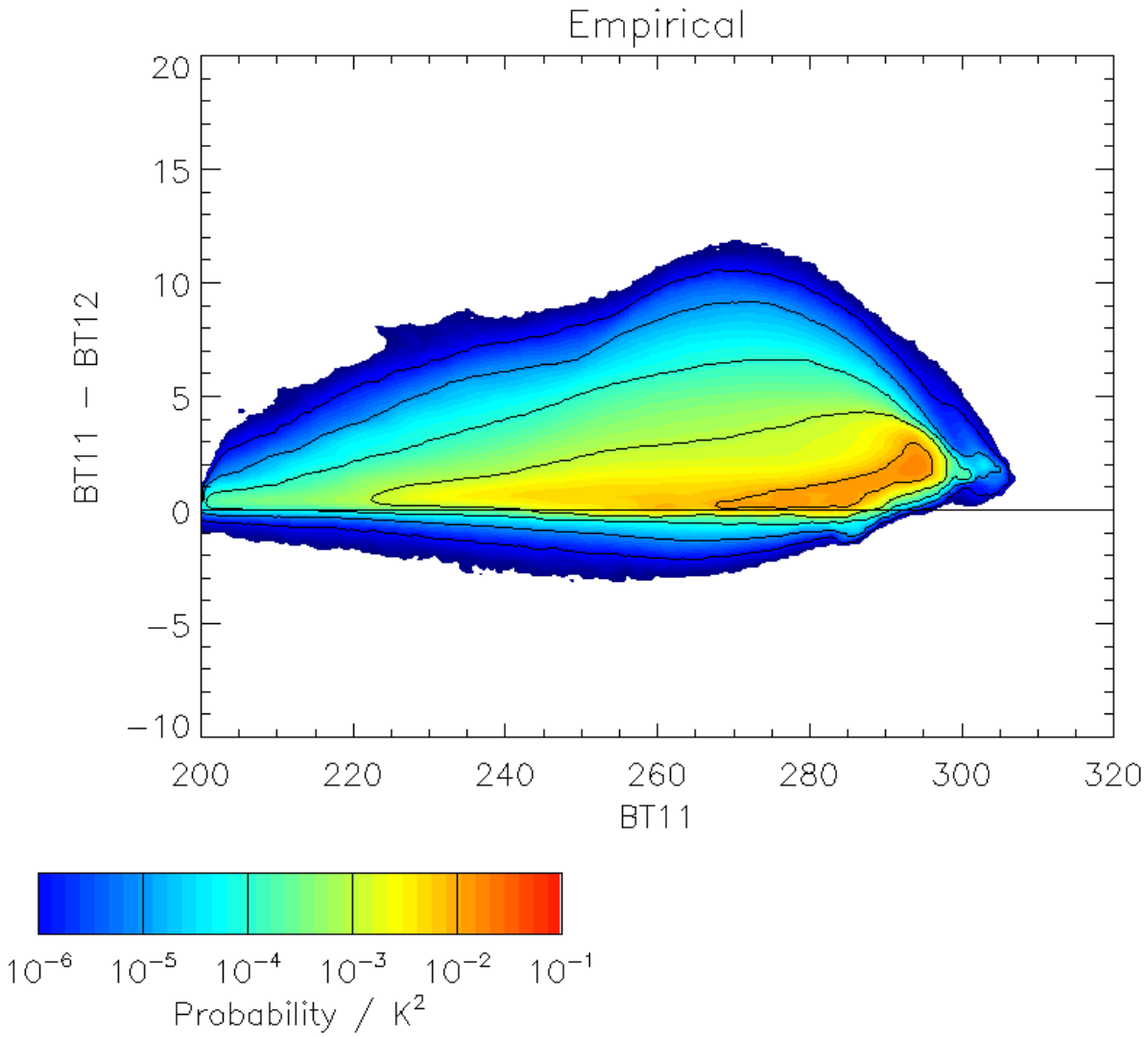


**Figure 19 As** Figure 16 **for BT-BT12 difference.**

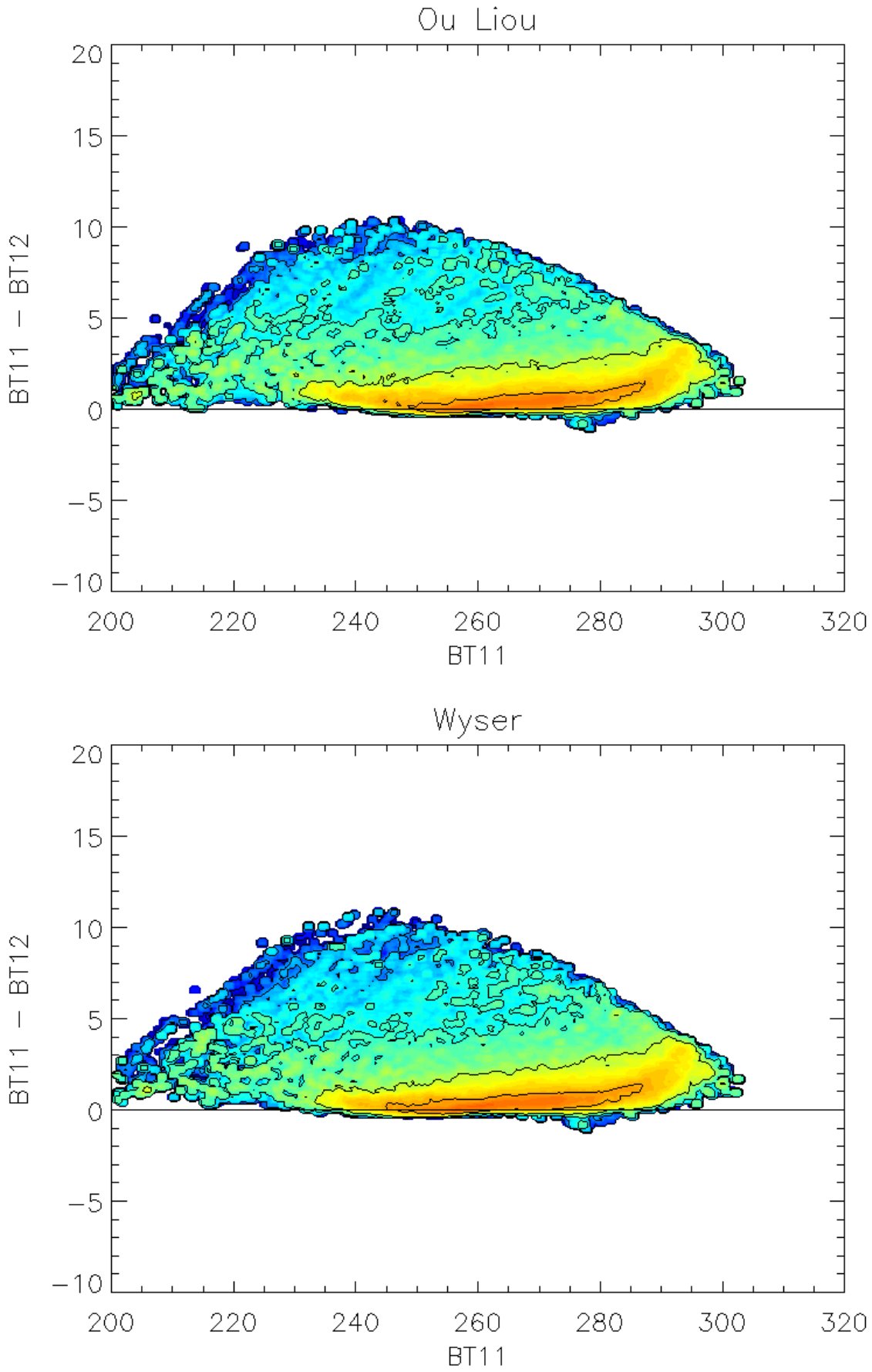


**Figure 20 As Figure 17 for BT11-BT12 difference.**

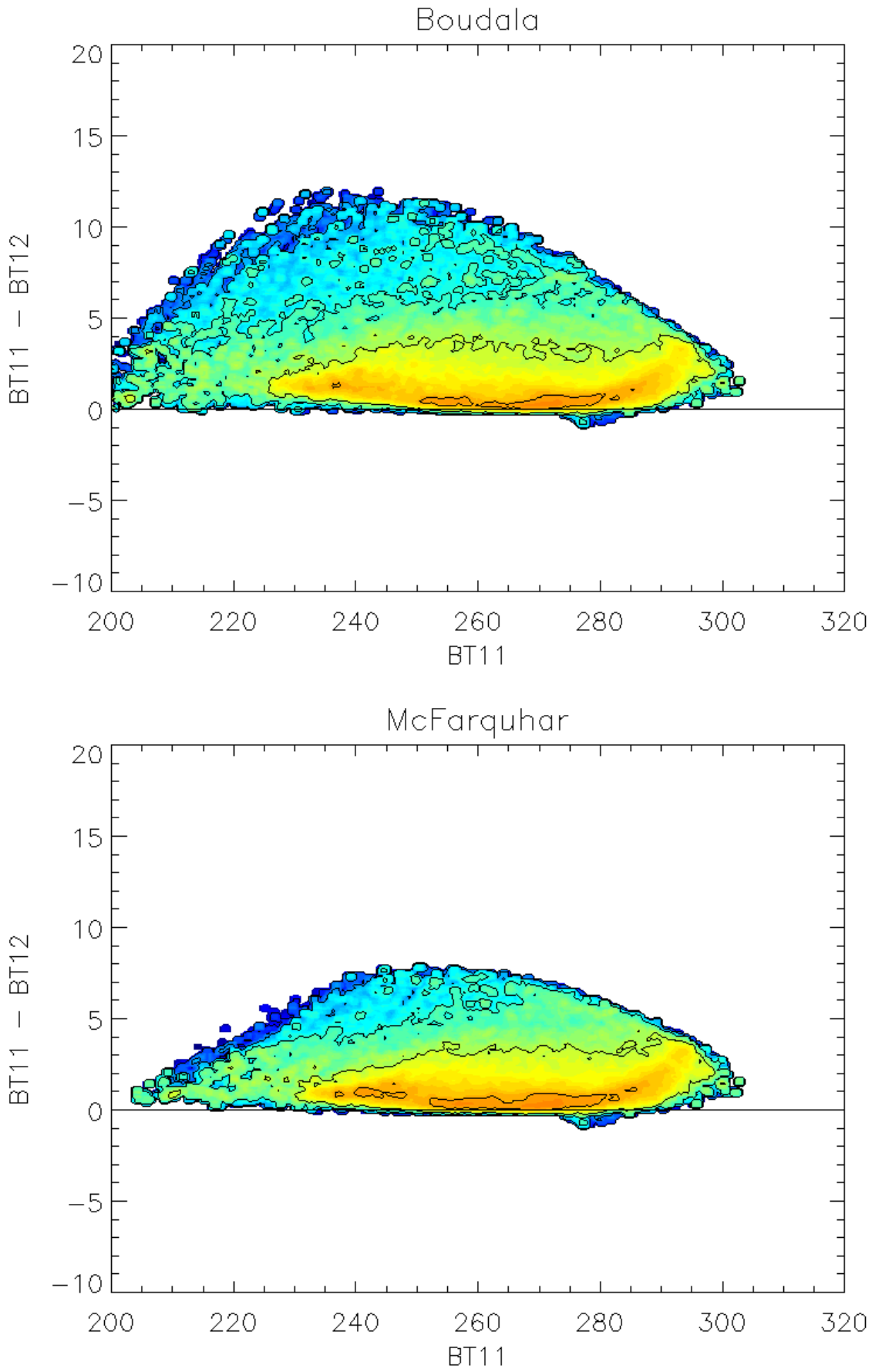


**Figure 21 As Figure 18 for BT11-BT12 difference**

## *4.3 Case Study*

### 4.3.1 Satellite observations

An ATSR-2 image, shown in Figure 22 (from 06:46am 04/10/1997; 11°N, 126°W), was chosen to compare individual RT8C simulations with observed data. The chosen image contains examples of both thin cirrus and water clouds. Both are relatively simple (i.e. single layer) cases which should be relatively easy to model. Three regions are marked, where both the nadir view and forward view (not shown) correspond to a single layer of cloud. Region A is water cloud at an altitude of 3 km. Regions B and C are cirrus cloud at altitudes of 15 km and 17 km respectively. Height estimation is done using the dual view capability and maximum cross-correlation, and is precise to ±1 km.

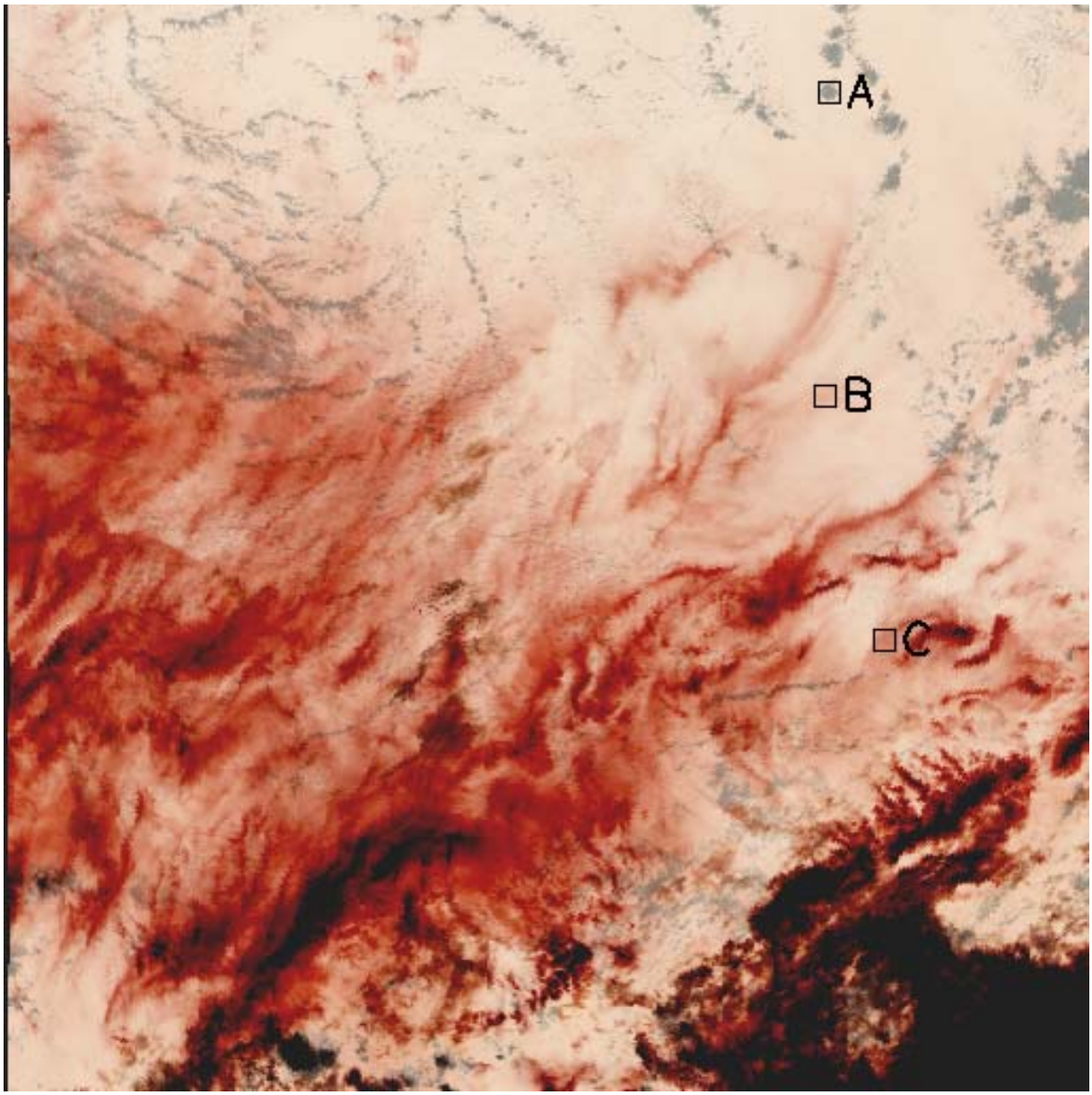


**Figure 22 False colour ATSR2 image from 06:46am 04/10/1997 (11°N, 126°W). Channels are: 3.7 micron (red), 11 micron (green), 12 micron (blue). Range is such that pixels colder than 270 K are black, warmer than 300 K are white. Height retrieval using forward view image (not shown) indicates red clouds have a heights between 15 and 17 km and grey clouds have a height 3±1 km. Regions A, B, and C are discussed in text.**

### 4.3.2 Profile data

To simulate the observations, knowledge of the atmospheric state is required. The profiles of atmospheric humidity and temperature were taken from the ECMWF operational data archive at BADC (badc.nerc.ac.uk). At the required time, profile data were available on 15 pressure levels (10, 30, 50, 70, 100, 150, 200, 250, 300, 400, 500, 700, 850, 1000 mbar) and a 2.5 degree grid.

These profiles are interpolated to the location (pixel) of interest and then interpolated to the 43 RTTOV pressure levels for both standard RTTOV and RT8C calculations.

### 4.3.3 Cloud top height data and assumptions

Cloud top heights were determined using the dual view capability of ATSR with code supplied by S. Matthiesen (University of Edinburgh). The procedure is to find the along-track offset between the apparent location of the cloud in the forward and nadir views, based on maximum cross-correlation, and the to convert this to a height estimated using the satellite viewing geometry. Because of the resolution of the nadir view, the error in altitude is at best ±1 km.

The clouds are assumed to occupy a single RTTOV level and occupy 100% of the field of view. Simulations are run using a range of cloud liquid/ice water contents, the four different parameterisations of particle size for ice clouds, and (for ice clouds) both hexagonal and aggregate crystal habits.

### 4.3.4 Observation-simulation comparison

The 'true' brightness temperature is taken as the average BT in each channel for a 3x3 box of pixels centered on the pixel of interest. The model (RT8C / DISORT) error is taken as the difference between the simulated BT and the average observed BT.

To create a single statistic describing the closeness of fit of observed and simulated BTs, we use a root mean square error (RMSE) calculated as:

$$rmse = \sqrt{\frac{1}{5}\sum_{i=1}^{6}\left(x_i - \bar{y}_i\right)^2}$$

where $x_i$ is the simulated BT in channel *i* and $\bar{y}_i$ is the average observed BT in channel *i*.

To quantify the uncertainty in the estimate of 'true' BTs, an RMSE value is also calculated from the observations across the 3x3 box as:

$$\sqrt{\frac{1}{53}\sum_{i=1}^{6}\sum_{j=1}^{9}\left(y_i^j - \bar{y}_i\right)^2}$$

where $y_i^j$ is the BT in channel *i* of pixel *j* (*j* runs from 1 to 9 across the 3x3 pixel box).

Since we don't have independent estimates of the cloud liquid or ice water content for the simulation, the value of these that minimizes the RMSE is used to define the best simulation for comparison with the observed BTs. A range of cloud top heights around the stereoscopic estimate is also simulated.

### Case A (Water cloud)

Example results are shown in Table 13. Both RT8C and DISORT give good matches with the observations when the cloud height is assumed to be 2.1 km, although the cloud water content is 3.5x higher when RT8C is used. (The RT8C water content is actually at the minimum value for which the

RT8C simulations have "saturated" – i.e., the cloud is effectively opaque, and greater CLW content barely affects the simulated temperatures). The main improvement seen when using DISORT is that both views (forward and nadir) are simultaneously well matched, while there is a ~0.5K bias between them in the RT8C results; for this reason, a better "best" RMSE is obtained with DISORT. DISORT also seems better able to fit the 3.7 μm channel simultaneously with the others.

| | Height | Water content | Nadir | | | Forward | | | RMSE |
|---|---|---|---|---|---|---|---|---|---|
| | | | 12.04 | 10.85 | 3.74 | 12.04 | 10.85 | 3.74 | |
| Observed | 3.0 | | 285.30 | 286.40 | 285.79 | 283.26 | 284.88 | 284.70 | 0.19 |
| Clear-sky | | 0 | -6.21 | -8.22 | -12.09 | -4.64 | -6.54 | -11.27 | |
| ***RT8C*** | ***2.1*** | ***$5.00\times10^{-4}$*** | ***-0.03*** | ***-0.11*** | ***-0.87*** | ***-0.65*** | ***-0.63*** | ***-1.13*** | ***0.62*** |
| RT8C | 3.1 | $6.83\times10^{-5}$ | 1.80 | 1.26 | -2.77 | 1.70 | 1.93 | -0.04 | 1.95 |
| RT8C | 4.3 | $3.01\times10^{-5}$ | 1.89 | 0.39 | -5.81 | 3.75 | 3.24 | -2.29 | 3.59 |
| ***DISORT*** | ***2.1*** | ***$1.41\times10^{-4}$*** | ***0.34*** | ***0.24*** | ***-0.69*** | ***-0.13*** | ***0.07*** | ***0.01*** | ***0.34*** |
| DISORT | 3.1 | $4.83\times10^{-5}$ | 1.26 | 0.50 | -3.10 | 1.90 | 2.06 | 0.26 | 1.93 |
| DISORT | 4.3 | $2.47\times10^{-5}$ | 1.31 | -0.19 | -5.68 | 3.66 | 3.17 | -1.43 | 3.37 |

**Table 13 Results of modelling cloud in Region A of Figure 22. Observed row shows actual brightness temperatures, other rows show error (modelled BT – observed BT). The best assumption RMSE for each model is the row in bold italic font; the other rows are the best fit with respect to CLW at other simulations heights.**

## Case B (Thin cirrus)

Refer to Table 14 for results. In all cases (both RT8C and DISORT, all heights, all cirrus models) at nadir the optimal modelled 12 micron BT is ~1 K warmer than the observed, the 11 micron is very close, and the 3.7 micron BT is ~1K colder than the observed. In the forward view a similar pattern occurs, but offset such that the modelled BTs are colder in comparison with the observed BT than is the case at nadir. This affects the RT8C results more than the DISORT results. The optimal RMSEs achieved by varying the CIW at the different heights are about 1 K, greater than for the water cloud.

The RT8C simulations were run using both hexagonal and aggregate ice crystal models. The hexagonal model consistently gave slightly better agreement with the observations, irrespective of height and particle size parameterisation.

Full scattering parameters were not available for the hexagonal model, so DISORT was run using only the aggregate crystal model. The DISORT BTs are overall in slightly better agreement with the observations than either set of RT8C BTs.

Comparing the four effective particle size parameterizations, there are only very small differences between them in terms of the RMSE achieved. The McFarquhar et al. model with DISORT gave the closest match, which appears to be a result consistent with the verification of cloudy radiance distributions in the previous section.

Although similar RMSEs were achieved, the CIW content at which the optimal simulation was achieved varies markedly, with the McFarquhar particle size parameterisation giving the highest CIW, and the Boudala parameterisation giving a CIW about half as large.

| | Height | Ice content | Nadir | | | Forward | | | RMSE |
|---|---|---|---|---|---|---|---|---|---|
| | | | 12.04 | 10.85 | 3.74 | 12.04 | 10.85 | 3.74 | |
| Observed | 15.1 | | 286.01 | 289.44 | 296.01 | 278.53 | 282.76 | 292.80 | 0.29 |
| Clear-sky | | | -3.23 | -3.37 | -1.57 | -6.60 | -6.27 | -2.74 | |
| Ou and Liou | | | | | | | | | |
| RT8C hex | 14.5 | $5.04\times10^{-6}$ | 1.01 | 0.24 | -0.83 | 0.07 | -0.52 | -1.52 | 0.93 |
| RT8C hex | 15.5 | $5.33\times10^{-6}$ | 1.00 | 0.21 | -0.86 | 0.10 | -0.55 | -1.58 | 0.96 |
| RT8C hex | 16.5 | $5.60\times10^{-6}$ | 1.00 | 0.19 | -0.88 | 0.12 | -0.57 | -1.62 | 0.98 |
| RT8C agg | 14.5 | $5.66\times10^{-6}$ | 1.06 | 0.16 | -0.92 | 0.16 | -0.65 | -1.67 | 1.02 |
| RT8C agg | 15.5 | $5.98\times10^{-6}$ | 1.05 | 0.13 | -0.95 | 0.18 | -0.68 | -1.72 | 1.04 |
| RT8C agg | 16.5 | $6.29\times10^{-6}$ | 1.05 | 0.10 | -0.97 | 0.20 | -0.70 | -1.75 | 1.06 |
| DISORT | 14.5 | $5.46\times10^{-6}$ | 1.03 | 0.06 | -0.82 | 0.28 | -0.69 | -1.30 | 0.89 |
| DISORT | 15.5 | $5.79\times10^{-6}$ | 1.04 | 0.05 | -0.85 | 0.32 | -0.70 | -1.35 | 0.92 |
| DISORT | 16.5 | $6.08\times10^{-6}$ | 1.03 | 0.02 | -0.88 | 0.32 | -0.73 | -1.40 | 0.94 |
| Wyser | | | | | | | | | |
| RT8C hex | 14.5 | $4.93\times10^{-6}$ | 1.01 | 0.23 | -0.84 | 0.08 | -0.53 | -1.54 | 0.94 |
| RT8C hex | 15.5 | $4.42\times10^{-6}$ | 1.03 | 0.17 | -0.92 | 0.14 | -0.61 | -1.67 | 1.01 |
| RT8C hex | 16.5 | $4.32\times10^{-6}$ | 1.03 | 0.12 | -0.96 | 0.17 | -0.67 | -1.74 | 1.05 |
| RT8C agg | 14.5 | $5.63\times10^{-6}$ | 1.06 | 0.16 | -0.92 | 0.16 | -0.65 | -1.67 | 1.02 |
| RT8C agg | 15.5 | $4.98\times10^{-6}$ | 1.08 | 0.10 | -1.00 | 0.22 | -0.73 | -1.81 | 1.10 |
| RT8C agg | 16.5 | $4.83\times10^{-6}$ | 1.08 | 0.05 | -1.04 | 0.25 | -0.78 | -1.87 | 1.14 |
| DISORT | 14.5 | $5.39\times10^{-6}$ | 1.04 | 0.06 | -0.82 | 0.29 | -0.70 | -1.30 | 0.90 |
| DISORT | 15.5 | $4.77\times10^{-6}$ | 1.05 | -0.01 | -0.89 | 0.33 | -0.79 | -1.42 | 0.96 |
| DISORT | 16.5 | $4.66\times10^{-6}$ | 1.06 | -0.04 | -0.93 | 0.37 | -0.82 | -1.48 | 1.00 |
| Boudala | | | | | | | | | |
| RT8C hex | 14.5 | $3.50\times10^{-6}$ | 1.07 | 0.16 | -0.94 | 0.17 | -0.65 | -1.71 | 1.04 |
| RT8C hex | 15.5 | $3.38\times10^{-6}$ | 1.07 | 0.10 | -0.99 | 0.21 | -0.72 | -1.80 | 1.09 |
| RT8C hex | 16.5 | $3.25\times10^{-6}$ | 1.09 | 0.06 | -1.04 | 0.26 | -0.77 | -1.87 | 1.13 |
| RT8C agg | 14.5 | $3.90\times10^{-6}$ | 1.10 | 0.08 | -1.03 | 0.21 | -0.77 | -1.85 | 1.13 |
| RT8C agg | 15.5 | $3.76\times10^{-6}$ | 1.10 | 0.04 | -1.07 | 0.26 | -0.82 | -1.92 | 1.17 |
| RT8C agg | 16.5 | $3.60\times10^{-6}$ | 1.11 | -0.01 | -1.11 | 0.28 | -0.88 | -1.99 | 1.20 |
| DISORT | 14.5 | $3.74\times10^{-6}$ | 1.07 | -0.02 | -0.90 | 0.35 | -0.82 | -1.41 | 0.97 |
| DISORT | 15.5 | $3.62\times10^{-6}$ | 1.08 | -0.06 | -0.94 | 0.40 | -0.86 | -1.49 | 1.02 |
| DISORT | 16.5 | $3.47\times10^{-6}$ | 1.10 | -0.09 | -0.98 | 0.44 | -0.91 | -1.55 | 1.06 |
| McFarquhar | | | | | | | | | |
| RT8C hex | 14.5 | $6.32\times10^{-6}$ | 0.98 | 0.29 | -0.75 | 0.03 | -0.44 | -1.39 | 0.86 |
| RT8C hex | 15.5 | $6.59\times10^{-6}$ | 0.98 | 0.27 | -0.79 | 0.07 | -0.46 | -1.45 | 0.89 |
| RT8C hex | 16.5 | $6.78\times10^{-6}$ | 0.98 | 0.24 | -0.82 | 0.09 | -0.49 | -1.51 | 0.92 |
| RT8C agg | 14.5 | $7.41\times10^{-6}$ | 1.04 | 0.23 | -0.82 | 0.12 | -0.54 | -1.50 | 0.93 |
| RT8C agg | 15.5 | $7.70\times10^{-6}$ | 1.04 | 0.19 | -0.85 | 0.15 | -0.57 | -1.57 | 0.96 |
| RT8C agg | 16.5 | $7.92\times10^{-6}$ | 1.04 | 0.17 | -0.89 | 0.18 | -0.60 | -1.62 | 0.99 |
| DISORT | 14.5 | $7.09\times10^{-6}$ | 1.01 | 0.13 | -0.75 | 0.24 | -0.58 | -1.21 | 0.83 |
| DISORT | 15.5 | $7.36\times10^{-6}$ | 1.00 | 0.10 | -0.79 | 0.26 | -0.62 | -1.28 | 0.87 |
| DISORT | 16.5 | $7.57\times10^{-6}$ | 1.00 | 0.07 | -0.83 | 0.27 | -0.66 | -1.34 | 0.89 |

**Table 14 As Table 13 for Region B. Simulations run using the four different ice particle size parameterizations and both hexagonal and aggregate scattering properties in RT8C. Only aggregate scattering properties were available in DISORT.**

## Case C

Case C follows similar patterns to Case B, except the simulation-observation differences are significantly larger (RMSE ~2 K, in stead of ~1 K). This is presumably due to the cloud at C being much thicker and less uniform than B. Refer to Table 15.

| | Height | Water content | Nadir | | | Forward | | | RMSE |
|---|---|---|---|---|---|---|---|---|---|
| | | | 12.04 | 10.85 | 3.74 | 12.04 | 10.85 | 3.74 | |
| Observed | 17.5 | | 278.72 | 282.47 | 292.92 | 268.44 | 272.88 | 288.29 | 0.49 |
| Clear-sky | | | -9.95 | -9.82 | -4.54 | -16.22 | -15.67 | -7.17 | |
| Ou and Liou | | | | | | | | | |
| RT8C hex | 16.5 | $1.54\times10^{-5}$ | 1.32 | -0.26 | -2.65 | 1.08 | -0.82 | -4.12 | 2.35 |
| RT8C hex | 17.5 | $1.80\times10^{-5}$ | 1.32 | -0.28 | -2.68 | 1.11 | -0.83 | -4.16 | 2.37 |
| RT8C hex | 18.7 | $2.03\times10^{-5}$ | 1.32 | -0.25 | -2.65 | 1.07 | -0.82 | -4.11 | 2.35 |
| RT8C agg | 16.5 | $1.74\times10^{-5}$ | 1.47 | -0.46 | -2.88 | 1.29 | -1.13 | -4.48 | 2.60 |
| RT8C agg | 17.5 | $2.03\times10^{-5}$ | 1.45 | -0.49 | -2.90 | 1.30 | -1.16 | -4.52 | 2.62 |
| RT8C agg | 18.7 | $2.28\times10^{-5}$ | 1.46 | -0.47 | -2.88 | 1.27 | -1.14 | -4.48 | 2.59 |
| DISORT | 16.5 | $1.67\times10^{-5}$ | 1.43 | -0.67 | -2.54 | 1.56 | -1.27 | -3.53 | 2.26 |
| DISORT | 17.5 | $1.96\times10^{-5}$ | 1.42 | -0.70 | -2.56 | 1.56 | -1.30 | -3.57 | 2.28 |
| DISORT | 18.7 | $2.20\times10^{-5}$ | 1.43 | -0.67 | -2.53 | 1.54 | -1.27 | -3.52 | 2.25 |
| Wyser | | | | | | | | | |
| RT8C hex | 16.5 | $1.25\times10^{-5}$ | 1.41 | -0.37 | -2.83 | 1.21 | -0.99 | -4.39 | 2.53 |
| RT8C hex | 17.5 | $1.43\times10^{-5}$ | 1.42 | -0.41 | -2.87 | 1.25 | -1.03 | -4.46 | 2.57 |
| RT8C hex | 18.7 | $1.64\times10^{-5}$ | 1.41 | -0.38 | -2.83 | 1.20 | -1.00 | -4.39 | 2.53 |
| RT8C agg | 16.5 | $1.41\times10^{-5}$ | 1.53 | -0.57 | -3.05 | 1.39 | -1.29 | -4.75 | 2.76 |
| RT8C agg | 17.5 | $1.60\times10^{-5}$ | 1.54 | -0.61 | -3.09 | 1.42 | -1.33 | -4.81 | 2.80 |
| RT8C agg | 18.7 | $1.85\times10^{-5}$ | 1.54 | -0.56 | -3.05 | 1.39 | -1.28 | -4.75 | 2.76 |
| DISORT | 16.5 | $1.35\times10^{-5}$ | 1.50 | -0.79 | -2.66 | 1.67 | -1.44 | -3.71 | 2.39 |
| DISORT | 17.5 | $1.54\times10^{-5}$ | 1.52 | -0.81 | -2.69 | 1.72 | -1.46 | -3.76 | 2.43 |
| DISORT | 18.7 | $1.78\times10^{-5}$ | 1.53 | -0.76 | -2.65 | 1.70 | -1.40 | -3.69 | 2.38 |
| Boudala | | | | | | | | | |
| RT8C hex | 16.5 | $9.57\times10^{-6}$ | 1.52 | -0.55 | -3.03 | 1.37 | -1.26 | -4.72 | 2.74 |
| RT8C hex | 17.5 | $1.09\times10^{-5}$ | 1.54 | -0.59 | -3.07 | 1.42 | -1.30 | -4.79 | 2.79 |
| RT8C hex | 18.7 | $1.26\times10^{-5}$ | 1.53 | -0.55 | -3.03 | 1.37 | -1.26 | -4.72 | 2.74 |
| RT8C agg | 16.5 | $1.07\times10^{-5}$ | 1.61 | -0.71 | -3.23 | 1.49 | -1.51 | -5.05 | 2.95 |
| RT8C agg | 17.5 | $1.21\times10^{-5}$ | 1.61 | -0.76 | -3.27 | 1.53 | -1.55 | -5.11 | 2.99 |
| RT8C agg | 18.7 | $1.40\times10^{-5}$ | 1.60 | -0.71 | -3.23 | 1.49 | -1.51 | -5.05 | 2.95 |
| DISORT | 16.5 | $1.02\times10^{-5}$ | 1.58 | -0.93 | -2.79 | 1.80 | -1.65 | -3.90 | 2.54 |
| DISORT | 17.5 | $1.16\times10^{-5}$ | 1.61 | -0.94 | -2.82 | 1.87 | -1.66 | -3.94 | 2.58 |
| DISORT | 18.7 | $1.35\times10^{-5}$ | 1.60 | -0.91 | -2.78 | 1.82 | -1.63 | -3.88 | 2.54 |
| McFarquhar | | | | | | | | | |
| RT8C hex | 16.5 | $2.39\times10^{-5}$ | 1.18 | 0.02 | -2.23 | 0.86 | -0.41 | -3.44 | 1.95 |
| RT8C hex | 17.5 | $2.78\times10^{-5}$ | 1.18 | -0.01 | -2.27 | 0.89 | -0.42 | -3.49 | 1.98 |
| RT8C hex | 18.7 | $3.06\times10^{-5}$ | 1.19 | 0.01 | -2.26 | 0.88 | -0.42 | -3.47 | 1.98 |
| RT8C agg | 16.5 | $2.84\times10^{-5}$ | 1.33 | -0.13 | -2.36 | 1.09 | -0.63 | -3.65 | 2.11 |
| RT8C agg | 17.5 | $3.31\times10^{-5}$ | 1.33 | -0.16 | -2.40 | 1.11 | -0.66 | -3.70 | 2.14 |
| RT8C agg | 18.7 | $3.64\times10^{-5}$ | 1.34 | -0.15 | -2.40 | 1.10 | -0.66 | -3.70 | 2.14 |
| DISORT | 16.5 | $2.70\times10^{-5}$ | 1.23 | -0.39 | -2.25 | 1.22 | -0.85 | -3.19 | 1.95 |
| DISORT | 17.5 | $3.15\times10^{-5}$ | 1.23 | -0.41 | -2.28 | 1.24 | -0.87 | -3.23 | 1.98 |
| DISORT | 18.7 | $3.47\times10^{-5}$ | 1.24 | -0.40 | -2.23 | 1.23 | -0.87 | -3.13 | 1.94 |

**Table 15 As Table 13 for Region C. Simulations run using the four different ice particle size parameterizations and both hexagonal and aggregate scattering properties in RT8C. Only aggregate scattering properties were available in DISORT.**

## 4.4 Conclusions (Section 4)

The statistical distributions show the effects of ignoring scattering through the lack of clouds with BT11 > BT3. This is a characteristic of fog and low stratus where the emissivity is greater at 11 microns than 3 microns. However, in the absorption only approximation (emission + transmission = 1) the lower emission at 3.7 μm is counteracted with transmitted surface radiance which significantly increases BT3 due to the extreme non-linearity of the Planck function.

For opaque ice clouds (i.e. BT11 < 240 K) there is a significant difference in the distribution of BTs. In the simulations the minimum BT3-BT11 increases as BT11 decreases (to about 10 K at BT11=200 K), while in the observations negative values are always possible. This is held to be another consequence of the neglect of scattering.

There was some evidence from the simulated distributions that the McFarquhar parameterisation of particle size distribution is more effective for simulation of 3.7 μm cloudy radiances.

The limited case study involving cases is less conclusive, partly due to the unknown variables describing the clouds studied. The cloud height is estimated to about 1 km using stereo methods, but the clouds' physical and optical thicknesses are unknown. Errors in NWP profiles and SST no doubt also contribute to the discrepancies between observed and simulated BTs that cannot be removed by varying the column water content of the clouds. Nonetheless, the case study does support the suggestion that the McFarquhar parameterisation of particle size distribution is more effective for simulation of 3.7 μm cloudy radiances (for both the RT8C approximation and DISORT full scattering simulations).

## 4.5 References (section 4)

Boudala, F.S., Isaac, G.A., Fu, Q. & Cober, S.G., 2002 : Parameterization of effective ice particle size for high-latitude clouds. Int. J. Climatol., 22, 1267-1284.

McFarquhar, G.M., Iacobellis, S. & Somerville, R.C.J., 2003 : SCM simulations of tropical ice clouds using observationally based parameterizations of microphysics. J. Clim., 16, 1643-1664.

Ou S.-C. and K.-N. Liou 1995 Ice microphysics and climatic temperature feedback. Atmos. Res. 35 127-138.

Wyser, K., 1998: The effective radius in cirrus clouds. J. Clim., 11, 1793-1802.

## *Appendix A – Listings of scattering parameters from A Baran*

The listings below are for nine particle size distributions, taken from Fu 1996 J. Climate vol 9 2058-2082 and Mitchell et al. (1996) JAS vol 53 2967-88.

These size distributions (SDs) have effective radius, $r_e$, as follows:

| SD No | $r_e$ |
|---|---|
| 1 | 3.6 |
| 2 | 5.5 |
| 3 | 13.0 |
| 4 | 22.1 |
| 5 | 33.6 |
| 6 | 35.8 |
| 7 | 46.1 |
| 8 | 77.4 |
| 9 | 92.20 |

The definition of $r_e$ can be found in Francis et al. (1994) Quart J. Royal Met Soc vol 120 , 809-848.

λ=3.5

| SD | Cext ($Km^{-1}$) | $\omega_0$ | g |
|---|---|---|---|
| 1 | 0.430794 | 0.855569 | 8.097191231E-01 |
| 2 | 0.0982498 | 0.823330 | 8.020329535E-01 |
| 3 | 0.0801810 | 0.771502 | 8.124639172E-01 |
| 4 | 0.0199996 | 0.721459 | 8.316769173E-01 |
| 5 | 0.650121 | 0.648752 | 8.668827276E-01 |
| 6 | 0.121192 | 0.601199 | 8.952717460E-01 |
| 7 | 0.285361 | 0.565754 | 9.209314186E-01 |
| 8 | 0.656418 | 0.565308 | 9.303055696E-01 |
| 9 | 5.24966 | 0.554070 | 9.419930622E-01 |

λ=3.65

| SD | Cext ($Km^{-1}$) | $\omega_0$ | g |
|---|---|---|---|
| 1 | 0.426345 | 0.912533 | 8.144050680E-01 |
| 2 | 0.0985363 | 0.887075 | 8.105763177E-01 |
| 3 | 0.0803184 | 0.837859 | 8.236784772E-01 |
| 4 | 0.0199700 | 0.785510 | 8.432576670E-01 |
| 5 | 0.646992 | 0.711393 | 8.781420442E-01 |
| 6 | 0.120189 | 0.661555 | 9.040496690E-01 |
| 7 | 0.286251 | 0.618433 | 9.249652522E-01 |
| 8 | 0.653685 | 0.587839 | 9.331422954E-01 |
| 9 | 5.24270 | 0.566802 | 9.445566796E-01 |

λ=3.80

| SD | Cext ($Km^{-1}$) | $\omega_0$ | g |
|---|---|---|---|
| 1 | 0.424751 | 0.925949 | 8.483780020E-01 |
| 2 | 0.0994052 | 0.904072 | 8.479841192E-01 |
| 3 | 0.0810547 | 0.856998 | 8.562592114E-01 |
| 4 | 0.0200762 | 0.804763 | 8.683685692E-01 |

| | | | |
|---|---|---|---|
| 5 | 0.644870 | 0.729987 | 8.906132018E-01 |
| 6 | 0.119384 | 0.679914 | 9.094409190E-01 |
| 7 | 0.283784 | 0.633239 | 9.255289406E-01 |
| 8 | 0.652010 | 0.596635 | 9.354313079E-01 |
| 9 | 5.22126 | 0.571384 | 9.450247563E-01 |

λ=4.00

| SD | Cext ($Km^{-1}$) | $\omega_0$ | g |
|---|---|---|---|
| 1 | 0.442340 | 0.911040 | 8.770112222E-01 |
| 2 | 0.105096 | 0.888261 | 8.769203520E-01 |
| 3 | 0.0854300 | 0.840238 | 8.813857788E-01 |
| 4 | 0.0209711 | 0.787358 | 8.886617285E-01 |
| 5 | 0.663358 | 0.708086 | 9.024450161E-01 |
| 6 | 0.121510 | 0.653274 | 9.150150812E-01 |
| 7 | 0.287083 | 0.607810 | 9.274633223E-01 |
| 8 | 0.656303 | 0.581308 | 9.389173208E-01 |
| 9 | 5.24287 | 0.560078 | 9.476904750E-01 |

λ=4.25

| SD | Cext ($Km^{-1}$) | $\omega_0$ | g |
|---|---|---|---|
| 1 | 0.415680 | 0.874547 | 8.978464791E-01 |
| 2 | 0.100658 | 0.849369 | 8.983824538E-01 |
| 3 | 0.0831219 | 0.799953 | 9.004163795E-01 |
| 4 | 0.0206064 | 0.748097 | 9.042588020E-01 |
| 5 | 0.658240 | 0.669658 | 9.107043380E-01 |
| 6 | 0.120704 | 0.614339 | 9.168883915E-01 |
| 7 | 0.285410 | 0.574683 | 9.268821392E-01 |
| 8 | 0.655700 | 0.564837 | 9.409624383E-01 |
| 9 | 5.24435 | 0.550103 | 9.486965721E-01 |

λ=10.00

| SD | Cext ($Km^{-1}$) | $\omega_0$ | g |
|---|---|---|---|
| 1 | 0.123609 | 0.540059 | 8.998813386E-01 |
| 2 | 0.0388983 | 0.577817 | 9.239048665E-01 |
| 3 | 0.0427171 | 0.587472 | 9.431298686E-01 |
| 4 | 0.0129280 | 0.582515 | 9.550317128E-01 |
| 5 | 0.512341 | 0.572988 | 9.675537796E-01 |
| 6 | 0.102303 | 0.558978 | 9.744058567E-01 |
| 7 | 0.254145 | 0.541459 | 9.802169831E-01 |
| 8 | 0.621006 | 0.535935 | 9.817615106E-01 |
| 9 | 5.17559 | 0.532872 | 9.838316159E-01 |

λ=10.25

| SD | Cext ($Km^{-1}$) | $\omega_0$ | g |
|---|---|---|---|
| 1 | 0.113851 | 0.393957 | 8.983551489E-01 |
| 2 | 0.0351426 | 0.448675 | 9.262411054E-01 |
| 3 | 0.0389715 | 0.489804 | 9.485769397E-01 |
| 4 | 0.0119945 | 0.509261 | 9.612362534E-01 |
| 5 | 0.485422 | 0.525529 | 9.731440996E-01 |
| 6 | 0.0985933 | 0.527833 | 9.789966109E-01 |
| 7 | 0.249707 | 0.526007 | 9.832773989E-01 |

| | | | |
|---|---|---|---|
| 8 | 0.613130 | 0.523496 | 9.839469958E-01 |
| 9 | 5.13247 | 0.524304 | 9.853972204E-01 |

λ=10.50

| SD | Cext ($Km^{-1}$) | $\omega_0$ | g |
|---|---|---|---|
| 1 | 0.118707 | 0.264472 | 8.954725488E-01 |
| 2 | 0.0349282 | 0.321239 | 9.261639638E-01 |
| 3 | 0.0377178 | 0.387266 | 9.514765674E-01 |
| 4 | 0.0115322 | 0.430717 | 9.646324479E-01 |
| 5 | 0.464538 | 0.472086 | 9.757406675E-01 |
| 6 | 0.0946626 | 0.490941 | 9.808340443E-01 |
| 7 | 0.242730 | 0.505938 | 9.838308016E-01 |
| 8 | 0.604832 | 0.510593 | 9.836990002E-01 |
| 9 | 5.08391 | 0.515784 | 9.846983787E-01 |

λ=10.75

| SD | Cext ($Km^{-1}$) | $\omega_0$ | g |
|---|---|---|---|
| 1 | 0.150917 | 0.216633 | 8.805933242E-01 |
| 2 | 0.0418719 | 0.267191 | 9.163920358E-01 |
| 3 | 0.0422412 | 0.337200 | 9.448876171E-01 |
| 4 | 0.0123514 | 0.390526 | 9.593075339E-01 |
| 5 | 0.474906 | 0.446195 | 9.712647414E-01 |
| 6 | 0.0947060 | 0.475004 | 9.766341732E-01 |
| 7 | 0.240036 | 0.499963 | 9.793672106E-01 |
| 8 | 0.604639 | 0.508701 | 9.788089358E-01 |
| 9 | 5.07183 | 0.516836 | 9.797430118E-01 |

λ=11.00

| SD | Cext ($Km^{-1}$) | $\omega_0$ | g |
|---|---|---|---|
| 1 | 0.193204 | 0.238487 | 8.663870901E-01 |
| 2 | 0.0516143 | 0.285147 | 9.029689558E-01 |
| 3 | 0.0491924 | 0.347480 | 9.323683763E-01 |
| 4 | 0.0137487 | 0.397499 | 9.484205444E-01 |
| 5 | 0.502093 | 0.454203 | 9.627188687E-01 |
| 6 | 0.0973969 | 0.485187 | 9.692960733E-01 |
| 7 | 0.241799 | 0.510964 | 9.727569050E-01 |
| 8 | 0.610651 | 0.518119 | 9.722154729E-01 |
| 9 | 5.09274 | 0.526587 | 9.733469521E-01 |

λ=11.25

| SD | Cext ($Km^{-1}$) | $\omega_0$ | g |
|---|---|---|---|
| 1 | 0.224531 | 0.273481 | 8.531778592E-01 |
| 2 | 0.0587882 | 0.318125 | 8.910455600E-01 |
| 3 | 0.0544380 | 0.373332 | 9.214602855E-01 |
| 4 | 0.0148484 | 0.417557 | 9.389093366E-01 |
| 5 | 0.527211 | 0.469430 | 9.553910009E-01 |
| 6 | 0.100504 | 0.497995 | 9.631633833E-01 |
| 7 | 0.245863 | 0.521079 | 9.674145820E-01 |
| 8 | 0.617036 | 0.527145 | 9.669236526E-01 |
| 9 | 5.12331 | 0.535053 | 9.682447111E-01 |

λ=11.50

| SD | Cext ($Km^{-1}$) | $\omega_0$ | g |
|---|---|---|---|
| 1 | 0.248597 | 0.294919 | 8.440325691E-01 |
| 2 | 0.0643369 | 0.336955 | 8.822865064E-01 |
| 3 | 0.0583971 | 0.386994 | 9.132333928E-01 |
| 4 | 0.0156469 | 0.427578 | 9.316398315E-01 |
| 5 | 0.543022 | 0.476506 | 9.497248046E-01 |
| 6 | 0.102241 | 0.504362 | 9.584722561E-01 |
| 7 | 0.247468 | 0.526752 | 9.633510317E-01 |
| 8 | 0.621520 | 0.533156 | 9.628649712E-01 |
| 9 | 5.14126 | 0.540871 | 9.643414785E-01 |

λ=11.75

| SD | Cext ($Km^{-1}$) | $\omega_0$ | g |
|---|---|---|---|
| 1 | 0.267203 | 0.313738 | 8.368162505E-01 |
| 2 | 0.0688337 | 0.354164 | 8.755520839E-01 |
| 3 | 0.0617721 | 0.400226 | 9.067823622E-01 |
| 4 | 0.0163560 | 0.437479 | 9.257696071E-01 |
| 5 | 0.558517 | 0.483128 | 9.450172922E-01 |
| 6 | 0.104079 | 0.509513 | 9.545382531E-01 |
| 7 | 0.249277 | 0.530767 | 9.599698253E-01 |
| 8 | 0.625378 | 0.537205 | 9.594743917E-01 |
| 9 | 5.15628 | 0.544730 | 9.611202571E-01 |

λ=12.00

| SD | Cext ($Km^{-1}$) | $\omega_0$ | g |
|---|---|---|---|
| 1 | 0.280563 | 0.330099 | 8.295221640E-01 |
| 2 | 0.0717840 | 0.368729 | 8.687643006E-01 |
| 3 | 0.0638004 | 0.411599 | 9.006887806E-01 |
| 4 | 0.0167577 | 0.446255 | 9.204792631E-01 |
| 5 | 0.566613 | 0.489047 | 9.409697616E-01 |
| 6 | 0.104976 | 0.513908 | 9.512387391E-01 |
| 7 | 0.250414 | 0.533883 | 9.571004793E-01 |
| 8 | 0.627169 | 0.540576 | 9.566054936E-01 |
| 9 | 5.16352 | 0.547819 | 9.583883396E-01 |

λ=12.25

| SD | Cext ($Km^{-1}$) | $\omega_0$ | g |
|---|---|---|---|
| 1 | 0.291317 | 0.345841 | 8.235424743E-01 |
| 2 | 0.0742116 | 0.382261 | 8.629252892E-01 |
| 3 | 0.0654296 | 0.421746 | 8.952951755E-01 |
| 4 | 0.0170654 | 0.453772 | 9.157962041E-01 |
| 5 | 0.571807 | 0.493631 | 9.374979694E-01 |
| 6 | 0.105405 | 0.516993 | 9.485407368E-01 |
| 7 | 0.250888 | 0.535947 | 9.548523204E-01 |
| 8 | 0.627956 | 0.542967 | 9.543264009E-01 |
| 9 | 5.16465 | 0.549981 | 9.562498705E-01 |

λ=12.50

| SD | Cext ($Km^{-1}$) | $\omega_0$ | g |
|---|---|---|---|
| 1 | 0.300349 | 0.361827 | 8.184229421E-01 |
| 2 | 0.0765568 | 0.396549 | 8.581841641E-01 |
| 3 | 0.0674360 | 0.433373 | 8.910387726E-01 |
| 4 | 0.0175701 | 0.463103 | 9.120550517E-01 |
| 5 | 0.592302 | 0.500840 | 9.346019906E-01 |
| 6 | 0.111027 | 0.523927 | 9.459102065E-01 |
| 7 | 0.264409 | 0.541301 | 9.522812816E-01 |
| 8 | 0.639495 | 0.546008 | 9.521595162E-01 |
| 9 | 5.18709 | 0.551850 | 9.543845789E-01 |

λ=12.75

| SD | Cext ($Km^{-1}$) | $\omega_0$ | g |
|---|---|---|---|
| 1 | 0.302673 | 0.378353 | 8.143696280E-01 |
| 2 | 0.0774927 | 0.411763 | 8.547652836E-01 |
| 3 | 0.0682351 | 0.445171 | 8.877752624E-01 |
| 4 | 0.0177084 | 0.471451 | 9.090682348E-01 |
| 5 | 0.588235 | 0.503736 | 9.323968869E-01 |
| 6 | 0.107647 | 0.522589 | 9.446503265E-01 |
| 7 | 0.253290 | 0.538282 | 9.518773051E-01 |
| 8 | 0.632610 | 0.546161 | 9.512559206E-01 |
| 9 | 5.18496 | 0.552429 | 9.534814253E-01 |

λ=13.00

| SD | Cext ($Km^{-1}$) | $\omega_0$ | g |
|---|---|---|---|
| 1 | 0.308574 | 0.394657 | 8.112042972E-01 |
| 2 | 0.0792697 | 0.425823 | 8.513634866E-01 |
| 3 | 0.0696759 | 0.455905 | 8.843671775E-01 |
| 4 | 0.0180190 | 0.479328 | 9.060080300E-01 |
| 5 | 0.595117 | 0.507952 | 9.302453897E-01 |
| 6 | 0.108445 | 0.524677 | 9.432387197E-01 |
| 7 | 0.254058 | 0.538777 | 9.510083439E-01 |
| 8 | 0.634252 | 0.547103 | 9.502931217E-01 |
| 9 | 5.19113 | 0.552992 | 9.526933349E-01 |